

**1      *In situ* Electrosynthesis of Anthraquinone Electrolytes in Aqueous Flow Batteries**

2      Yan Jing,<sup>1§</sup> Min Wu,<sup>2§</sup> Andrew A. Wong,<sup>2</sup> Eric M. Fell,<sup>2</sup> Shijian Jin,<sup>2</sup> Daniel A. Pollack,<sup>3</sup> Emily  
3      F. Kerr,<sup>1</sup> Roy G. Gordon,<sup>\*,1,2</sup> Michael J. Aziz<sup>\*,2</sup>

4      <sup>1</sup> Department of Chemistry and Chemical Biology, Harvard University, Cambridge,  
5      Massachusetts 02138, United States

6      <sup>2</sup> John A. Paulson School of Engineering and Applied Sciences, Harvard University, Cambridge,  
7      Massachusetts 02138, United States

8      <sup>3</sup> Department of Physics, Harvard University, Cambridge, Massachusetts 02138, United States

9      <sup>§</sup> These authors contributed equally to this work.

10     \* Correspondence: [gordon@chemistry.harvard.edu](mailto:gordon@chemistry.harvard.edu); [maziz@harvard.edu](mailto:maziz@harvard.edu)

**11     Abstract**

12     We demonstrate the electrochemical oxidation of an anthracene derivative to a redox-active  
13     anthraquinone at room temperature in a flow cell without the use of hazardous oxidants or noble  
14     metal catalysts. The anthraquinone, generated *in situ*, was used as the active species in a flow  
15     battery electrolyte without further modification or purification. This potentially scalable, safe,  
16     green, and economical electrosynthetic method is also applied to another anthracene-based  
17     derivative and may be extended to other redox-active aromatics.

**18     Introduction**

19     Aqueous redox flow batteries (ARFBs) represent a class of devices for storing electrical energy  
20     that are especially well suited for large-scale stationary deployment.<sup>1, 2</sup> Vanadium redox flow  
21     batteries, the most developed ARFB technology, have been limited by the high and fluctuating  
22     price of vanadium.<sup>3</sup>

23     Anthraquinone-based aqueous redox flow batteries are considered as one class of the most  
24     promising alternatives to vanadium redox flow batteries because they can be composed of earth-  
25     abundant elements such as C, H, O, and N while providing comparable electrochemical  
26     performance.<sup>4-9</sup> However, reducing the production cost of anthraquinone-based electrolytes and

27 improving their chemical stability are two major challenges preventing them from being cost-  
28 competitive.<sup>9-14</sup> Many factors can influence the synthesis cost of an organic molecule, including  
29 the number, duration, complexity, and yields of the reaction steps, the reaction conditions (time,  
30 temperature, and pressure), solvent and precursor costs, the cost of waste disposal, and economies  
31 of scale. Likewise, a host of factors contributes to the stability, and by extension the long-term  
32 viability, of redox-active organics including the chemical structure, solvent conditions, applied  
33 potentials, and state of charge. Only through careful consideration of all of these factors can  
34 commercial-scale organic ARFBs be viable storage solutions. Therefore, not only is the  
35 development of a stable anthraquinone important, but the design of a potentially economical,  
36 scalable, and green synthetic route toward targeted molecules is equally significant.<sup>11, 15</sup>

37 Electrochemically-mediated synthesis (electrosynthesis) enables the replacement of hazardous  
38 oxidizing and reducing agents by electric current, or “clean” electrons, through an electrode and  
39 has attracted considerable attention for both laboratory and industrial applications in multiple  
40 fields of research.<sup>16-21</sup> Compared to traditional thermochemical synthesis, electrosynthesis can be  
41 significantly more environmentally benign due to reduced waste production and alternative  
42 chemicals consumed.<sup>22, 23</sup> However, the necessity of using specific solvents combined with  
43 supporting electrolytes, along with their subsequent separations, are some of the primary hurdles  
44 limiting the feasibility of electrosynthesis compared to thermochemical processes in many cases.<sup>16</sup>

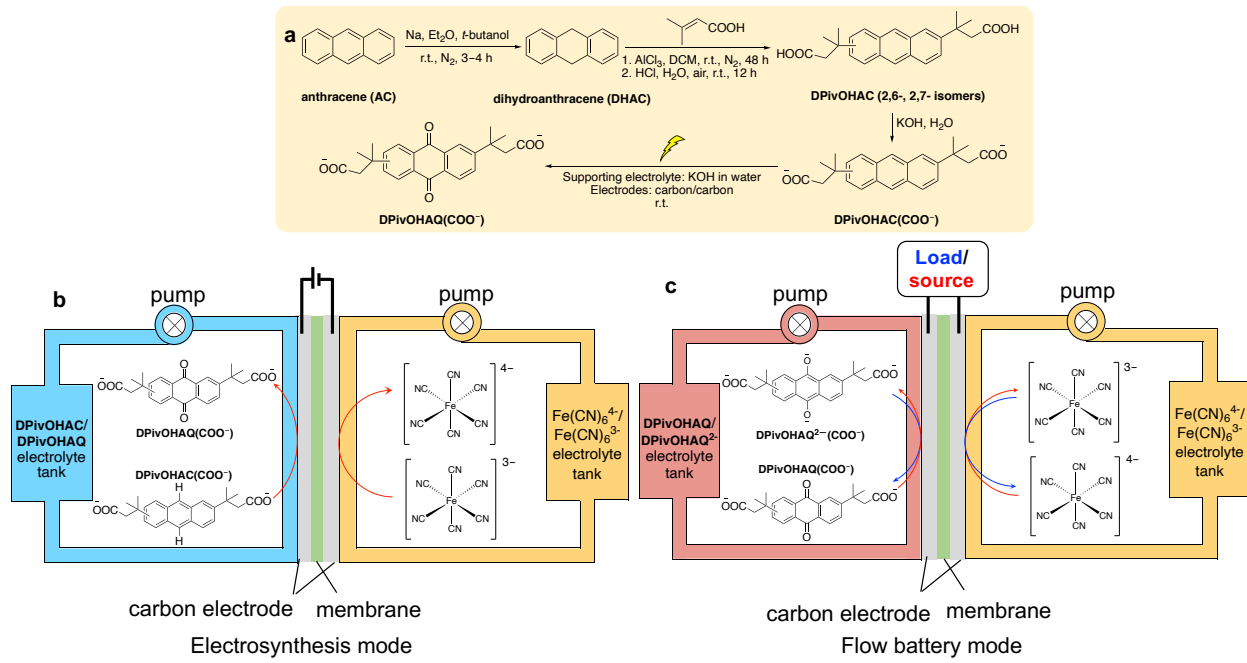
45 As an example, anthraquinone is typically produced from anthracene, an inexpensive and  
46 abundant component of coal tar and petroleum.<sup>24</sup> Typically, hazardous oxidants such as  
47 cerium(IV), chromium(VI), and vanadium(V) compounds dissolved in strong acids, sometimes at  
48 elevated temperatures, are used to facilitate this thermochemical conversion.<sup>25</sup> To minimize the  
49 use of hazardous materials, often these consumed oxidants are electrochemically regenerated and

50 reused for chemical oxidations,<sup>25-30</sup> that is, a mediated or indirect electrochemical oxidation.  
51 However, in both thermochemical conversion and mediated (indirect) electrochemical conversion,  
52 isolating anthraquinone from these hazardous solutions can be time- and capital-intensive. Electro-  
53 oxidations of anthracene and its derivatives at ~1 mM concentration have been performed  
54 previously; however, the low concentrations of anthracene substrates and poor selectivity of the  
55 reactions have prevented the method from being synthetically useful.<sup>31-36</sup>

56 Using a scalable flow cell setup,<sup>37</sup> we demonstrate the capability to electrochemically oxidize  
57 water-soluble anthracenes directly to anthraquinones in electrolytes without the use of strong  
58 oxidants or catalysts, producing the desired negolyte (negative electrolyte) and ferrocyanide  
59 posolyte (positive electrolyte) *in situ*. Compared to conventional thermochemical and  
60 electrochemical methods, the new method is safe and potentially inexpensive because it eliminates  
61 both the use of hazardous oxidants and the necessity of post-synthesis isolation of the products  
62 from the supporting electrolytes. Taking advantage of a flow cell and bulk electrolysis setup, the  
63 demonstrated electrosynthetic method is amenable to both continuous and batch processing.  
64 Furthermore, we confirmed that the electrosynthetic method can also be extended to other  
65 anthracene derivatives.

66 3,3'-(9,10-anthraquinone-diyl)bis(3-methylbutanoic acid) (**DPivOHAQ**) was recently reported  
67 as an extremely stable and potentially inexpensive negolyte active species for organic ARFBs.<sup>38</sup>  
68 However, the use of CrO<sub>3</sub> in the synthesis can be highly toxic and explosive if produced in large  
69 scale. Figure 1a shows the synthetic route for **DPivOHAQ** in three steps: 1) Through Birch  
70 reduction, anthracene (**AC**) is converted to 9,10-dihydroanthracene (**DHAC**) at room temperature  
71 (Figure S1). 2) After a Friedel–Crafts reaction and subsequent oxidation by air in one pot, two  
72 water-soluble groups are introduced and **DHAC** is re-oxidized to an **AC** derivative (Figure S2),

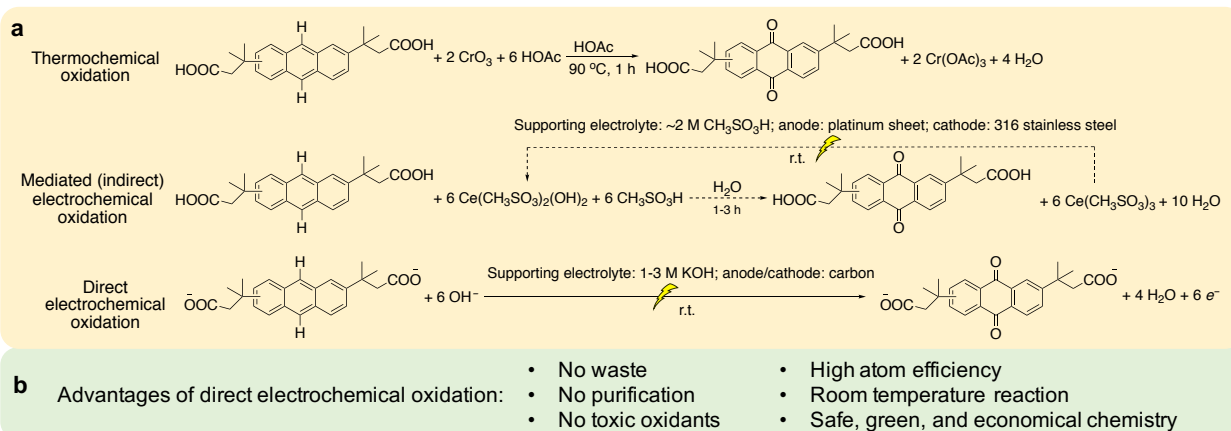
73 forming 3,3'-(anthracene-diyl)bis(3-methylbutanoic acid) (**DPivOHAC**). The **DPivOHAC**  
 74 powder was then dissolved in water by adding KOH to deprotonate the carboxylic acid groups. 3)  
 75 Lastly, **DPivOHAQ** negolyte active species is produced by electrochemical oxidation in an  
 76 aqueous electrolyte without the need for further purification. Figure 1b illustrates how  
 77 **DPivOHAQ** and ferrocyanide active species can be produced *in situ* in the flow cell's  
 78 electrosynthesis mode. These materials can directly serve as the active species in the negolyte and  
 79 the posolyte, respectively, of a flow battery in the same cell as illustrated in Figure 1c.  
 80



81 **Figure 1. Preparation of DPivOHAQ and the corresponding flow battery.** (a) The  
 82 **DPivOHAQ** synthetic route and conditions starting from anthracene. (b) The setup for  
 83 electrosynthesis of **DPivOHAQ** and ferrocyanide. (c) The flow battery setup with **DPivOHAQ**  
 84 negolyte (generated *in situ*) and ferrocyanide posolyte (generated *in situ*). **DPivOHAC**: 3,3'-  
 85 (anthracene-diyl)bis(3-methylbutanoic acid); **DPivOHAC(COO<sup>-</sup>)** is deprotonated **DPivOHAC**.  
 86 **DPivOHAQ**: 3,3'-(9,10-anthraquinone-diyl)bis(3-methylbutanoic acid); **DPivOHAQ(COO<sup>-</sup>)** is  
 87 deprotonated **DPivOHAQ**.

88 Figure 2a lists three different oxidation methods for **DPivOHAQ** synthesis. Conventionally,  
 89 anthracene derivatives can be chemically oxidized to their anthraquinone forms by oxidants such  
 90 as chromium oxide ( $\text{CrO}_3$ ) in strong acidic media at elevated temperature.<sup>38</sup> To minimize the use

91 of hazardous oxidants, the strategy of mediated electrochemical oxidation can be performed by  
 92 regenerating oxidants such as cerium(IV) compounds.<sup>26, 29</sup> However, in both of these  
 93 thermochemical and indirect electrochemical oxidation processes, tedious and expensive isolation  
 94 of anthraquinone-based products from oxidants and acids is required. Taking advantage of the high  
 95 solubility of **DPivOHAC** in base, we demonstrate a synthetic route via direct electrochemical  
 96 oxidation in alkaline electrolyte with a flow cell. This method allows the complete elimination of  
 97 hazardous oxidants and costly separation processes.



98

99 **Figure 2. Comparison of DPivOHAQ synthetic methods.** (a) Thermochemical, mediated  
 100 (indirect) electrochemical, and direct electrochemical oxidation reactions to synthesize  
 101 **DPivOHAQ**. (b) Advantages of direct electrochemical oxidation *in situ*.

102

## 103 Experimental

### 104 Cell hardware

105 Glassy carbon was used as the working electrode for all three-electrode cyclic voltammetry (CV)  
 106 tests with a 5 mm diameter glassy carbon working electrode, an Ag/AgCl reference electrode  
 107 (BASi, pre-soaked in 3 M NaCl solution), and a graphite counter electrode. Both undivided cell  
 108 and divided cell were built for electrosynthesis. Flow battery experiments were constructed with  
 109 cell hardware from Fuel Cell Tech (Albuquerque, NM) assembled into a zero-gap flow cell  
 110 configuration. Pyrosealed POCO graphite flow plates with serpentine flow patterns were used for

111 both electrodes. Each electrode comprised a 5 cm<sup>2</sup> geometric surface area covered by AvCarb  
112 HCBA woven carbon fiber without pretreatment, or Pt-coated Toray carbon paper without  
113 pretreatment. The membrane is pre-soaked (1 M KOH for 24 hours) Nafion 212.

114 *Undivided electrolytic cell setup (electrochemical oxidation vs. the HER)*

115 Working electrode: carbon felt, where **DPivOHAC(COO<sup>-</sup>)** was oxidized to **DPivOHAQ(COO<sup>-</sup>)**;  
116 counter electrode: carbon rod, where water was reduced to hydrogen gas. While the electrolyte  
117 was stirred, a constant potential (1.1 V vs. Ag/AgCl) was applied to the divided electrolytic cell  
118 until 120% of the required coulombs were extracted from the working electrode.

119 *Divided electrolytic cell setup (electrochemical oxidation vs. the ORR)*

120 Anode: Commercial AvCarb HCBA (woven carbon cloth), where **DPivOHAC(COO<sup>-</sup>)** was  
121 oxidized to **DPivOHAQ(COO<sup>-</sup>)**; cathode: platinum coated Toray carbon paper, where humidified  
122 air/oxygen was reduced to hydroxide. A constant voltage (1.8 V) was applied to the divided  
123 electrolytic cell until the current decreased to 2 mA/cm<sup>2</sup>. The number of extracted electrons was  
124 ~1.2 times higher than the theoretical value.

125 *Divided electrolytic cell setup (electrochemical oxidation vs. the reduction of ferricyanide)*

126 Anode: AvCarb HCBA (woven carbon cloth), where **DPivOHAC(COO<sup>-</sup>)** was oxidized to  
127 **DPivOHAQ(COO<sup>-</sup>)**; cathode: AvCarb HCBA (woven carbon cloth), where potassium  
128 ferricyanide was reduced to potassium ferrocyanide. A constant current density (20 mA/cm<sup>2</sup>) was  
129 applied to the divided cell for at most 1.5 hours with a 1.2 V voltage cutoff; when either time or  
130 voltage reached the limit, the potential was held (1.2 V vs. ferro-/ferricyanide) until the current  
131 decreased to 2 mA/cm<sup>2</sup>. The number of extracted electrons was ~1.2 times higher than the  
132 theoretical value.

133 An aliquot ( $\sim$ 250  $\mu$ L) was transferred from the as-prepared anolyte to an Eppendorf® tube  
134 (capacity: 1.5 mL) and acidified by a drop of concentrated HCl to obtain **DPivOHAQ** precipitate.  
135 The final **DPivOHAQ** precipitate was re-dissolved in DMSO-*d*<sub>6</sub> for <sup>1</sup>H NMR measurement. The  
136 yield was determined by peak integrations of spectrum. Faradaic efficiency (%) = yield (%) / 1.2.  
137 More detailed information can be found in the Supplementary information.

138 **Results and Discussion**

139 In an electrolytic cell, an anodic oxidation half reaction must be accompanied by a cathodic  
140 reduction half reaction. As shown in Table 1, we devise three different reduction half reactions to  
141 be coupled with direct **DPivOHAC** electrochemical oxidation, *i.e.*, the hydrogen evolution  
142 reaction (HER), the oxygen reduction reaction (ORR), and the  $\text{Fe}(\text{CN})_6^{3-}$  to  $\text{Fe}(\text{CN})_6^{4-}$  reduction  
143 reaction. The corresponding oxidation or reduction potentials for these reactions are listed in Table  
144 1.

145 For the electrochemical oxidation of **DPivOHAC** to **DPivOHAQ**, two cell types are used, as  
146 diagramed and described in Figures S3 and S4. A divided cell uses an ion exchange membrane to  
147 separate the two half reactions, resembling the architecture of traditional fuel cells and ARFBs.  
148 An undivided cell employs two electrodes suspended in electrolyte without the use of a membrane,  
149 reflecting a bulk electrolysis cell.

150 Comparing these three overall reactions, the first one paired with the HER requires the highest  
151 voltage; the second one paired with the ORR is known to have slow reaction kinetics and a high  
152 overpotential;<sup>39</sup> the third one paired with  $\text{Fe}(\text{CN})_6^{3-}$  to  $\text{Fe}(\text{CN})_6^{4-}$  reduction exhibits the lowest  
153 overall reaction cell voltage, suggesting the least amount of energy will be required for  
154 electrosynthesis. Another merit of the third reaction is the *in situ* generation of the desired negolyte  
155 active species (**DPivOHAQ**) and posolyte active species  $\text{Fe}(\text{CN})_6^{4-}$  simultaneously. The

156 disadvantage is that at least six equivalents of ferricyanide and hydroxide are used. Given the  
 157 similar reduction potentials of the ORR and of ferricyanide to ferrocyanide, an important direction  
 158 for future research is the concurrent reduction of oxygen and ferricyanide in order to achieve high  
 159 yields as well as lower ferricyanide usage. By using the same full cell configuration without  
 160 changing electrolyte reservoirs, carbon-based electrodes, or ion-exchange membranes, we can  
 161 immediately switch from electrosynthesis mode to flow battery mode for electrochemical energy  
 162 storage. In this configuration, neither hazardous oxidants nor purification steps are needed, nor is  
 163 waste generated. Furthermore, the reaction may proceed at room temperature with high atom  
 164 efficiency. The new synthesis is therefore potentially safe, green, economical, and scalable.

165 **Table 1.** Anodic, cathodic, and overall reactions for direct electrochemical oxidation.

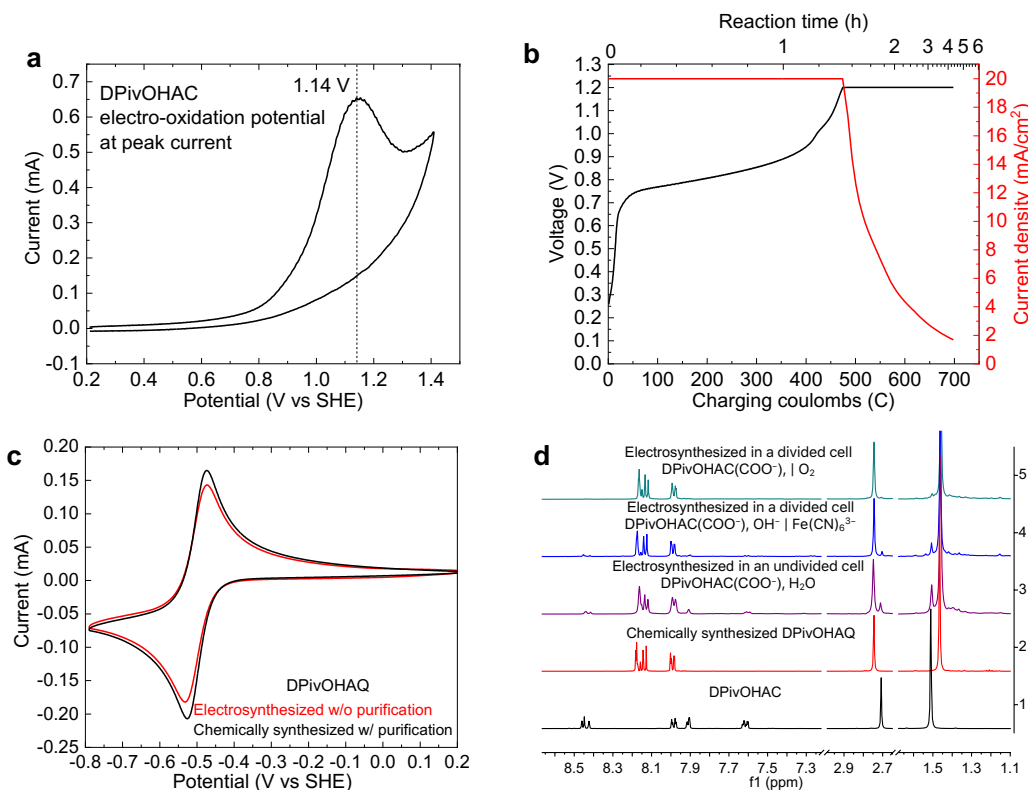
Reactions		Potential at pH 14 (V vs SHE) / Cell voltage (V)
Anodic	$\text{DPivOHAC}(\text{COO}^-) + 6 \text{OH}^- \longrightarrow \text{DPivOHAQ}(\text{COO}^-) + 4 \text{H}_2\text{O} + 6 e^-$	1.14*
Cathodic	$6 \text{H}_2\text{O} + 6 e^- \longrightarrow 3 \text{H}_2 + 6 \text{OH}^-$ (divided or undivided cell)	-0.83
	$1.5 \text{O}_2 + 6 e^- + 3 \text{H}_2\text{O} \longrightarrow 6 \text{OH}^-$ (divided or undivided cell)	0.40
	$6 \text{Fe}(\text{CN})_6^{3-} + 6 e^- \longrightarrow 6 \text{Fe}(\text{CN})_6^{4-}$ (divided cell)	0.44
Overall	$\text{DPivOHAC}(\text{COO}^-) + 2 \text{H}_2\text{O} \longrightarrow \text{DPivOHAQ}(\text{COO}^-) + 3 \text{H}_2$	1.97
	$\text{DPivOHAC}(\text{COO}^-) + 1.5 \text{O}_2 \longrightarrow \text{DPivOHAQ}(\text{COO}^-) + \text{H}_2\text{O}$	0.74
	$\text{DPivOHAC}(\text{COO}^-) + 6 \text{OH}^- + 6 \text{Fe}(\text{CN})_6^{3-} \longrightarrow \text{DPivOHAQ}(\text{COO}^-) + 6 \text{Fe}(\text{CN})_6^{4-} + 4 \text{H}_2\text{O}$	0.70

166 \*: The electro-oxidation potential at peak current

167 The cyclic voltammogram (CV) of **DPivOHAC** at pH 14 (Figure 3a) indicates a peak oxidation  
 168 current at 1.14 V vs. SHE. This value is more positive than the standard redox potential of 0.40 V  
 169 vs. SHE for the oxygen evolution reaction (OER), and we expect that the OER will be a major side  
 170 reaction of electrosynthesis.

171 We then assembled a flow cell with **DPivOHAC** as the anolyte and  $\text{K}_3\text{Fe}(\text{CN})_6$  as the catholyte.  
 172 Galvanostatic electrolysis with a potentiostatic hold after reaching a potential limit of 1.2 V was  
 173 performed for ~4.5 hours to complete the electrosynthesis. The OER side reaction, evidenced by

174 the observation of bubbles generated in the anolyte, precludes a faradaic efficiency of 100%. Thus,  
 175 the number of electrons extracted from the anolyte was ~1.2 times higher than the theoretical  
 176 number for complete conversion. A plateau appears at ~0.8 V against  $\text{K}_3\text{Fe}(\text{CN})_6$  (0.44 V vs. SHE)  
 177 in the voltage profile (Figure 3b).



178

179 **Figure 3. Electrosynthesis and characterization of DPivOHAQ.** (a) The cyclic voltammogram  
 180 (CV) of 0.1 M **DPivOHAC** in 1.0 M KCl + 1.0 M KOH aqueous solution. Scan rate: 0.1 V/s. (b)  
 181 The electrochemical oxidation was conducted by using a constant current (20 mA/cm<sup>2</sup>) with a  
 182 subsequent potential hold (1.2 V) until the current density decreased to 2 mA/cm<sup>2</sup>. (c) CV of  
 183 10 mM electro-synthesized **DPivOHAQ** (against  $\text{Fe}(\text{CN})_6^{3-}$ ) without purification and 10 mM  
 184 chemically synthesized **DPivOHAQ** with purification in 1 M KOH aqueous solutions,  
 185 respectively. Scan rate: 0.1 V/s. (d) <sup>1</sup>H NMR spectra of (bottom to top): chemically synthesized  
 186 **DPivOHAC** (black); chemically synthesized **DPivOHAQ** (red); electro-synthesized **DPivOHAQ**  
 187 in an undivided cell (purple), 17.3% of **DPivOHAC** remained unreacted according to the  
 188 integration, yield: 82.7%; electro-synthesized **DPivOHAQ** in a divided cell against  $\text{Fe}(\text{CN})_6^{3-}$   
 189 (blue), 7.0% of **DPivOHAC** remained unreacted according to the integration, yield: 93.0%;  
 190 electro-synthesized **DPivOHAQ** in a divided cell against  $\text{O}_2$  (green), 0 % of **DPivOHAC** remained  
 191 unreacted according to the integration, yield: 100%. The deuterated solvent is  $\text{DMSO}-d_6$ , and the  
 192 solvent peaks (DMSO and  $\text{H}_2\text{O}$ ) were removed to better display the peaks of interest. The

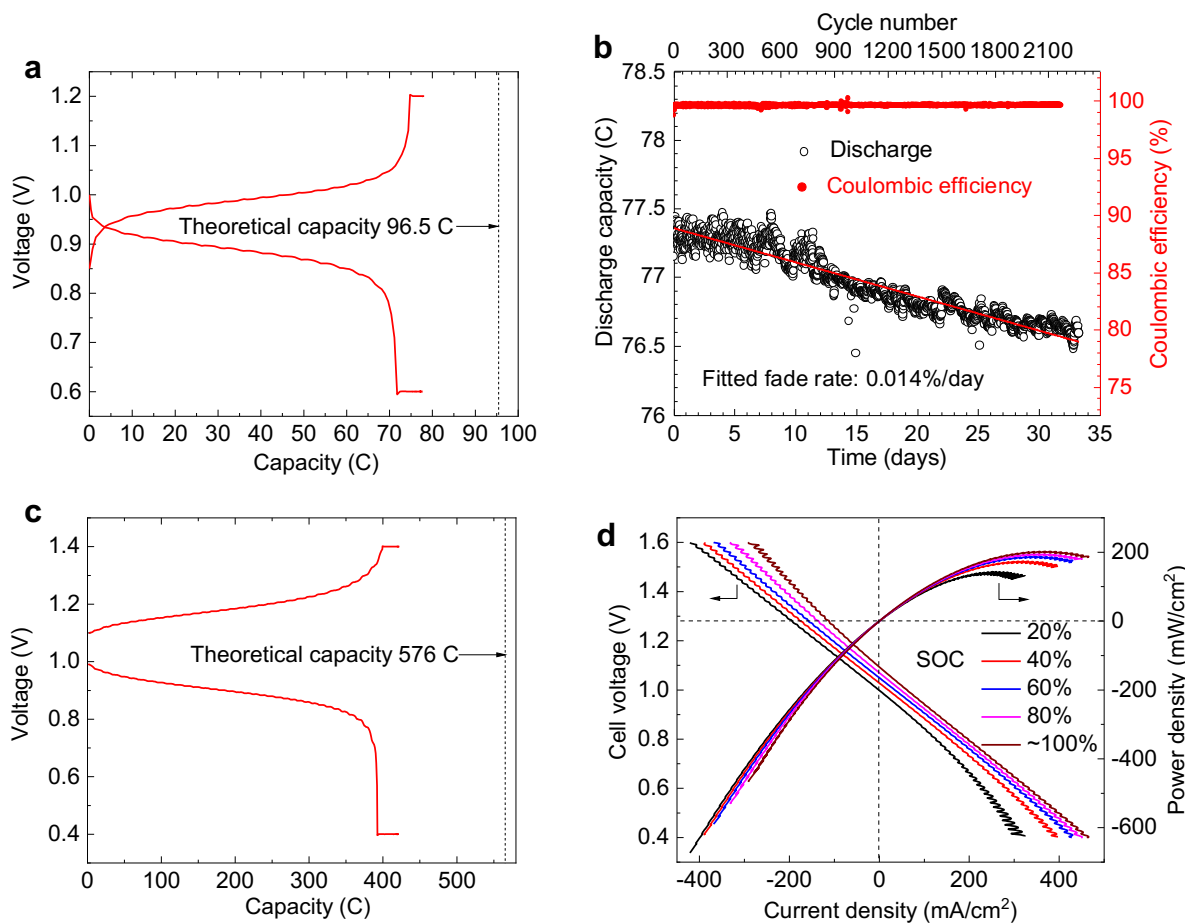
193 electrosynthetic details are described under the headings **Electrosynthesis I, II, and III** in the  
194 Supporting Information.

195

196 We compared the CV of **DPivOHAQ** produced by electrosynthesis against the reduction of  
197  $\text{Fe}(\text{CN})_6^{3-}$  to that of the chemically synthesized product at the same concentration to verify that  
198 the reaction products are the same regardless of the synthetic procedure employed (Figure 3c). The  
199 two CV curves show identical redox peaks and similar peak currents, indicating a high-yield  
200 electrosynthesis process.  $^1\text{H}$  nuclear magnetic resonance (NMR) spectroscopy was used to further  
201 examine the structure of electrosynthesized **DPivOHAQ** when using either a divided or undivided  
202 cell (Figure S3) and to compare the spectra with those of the starting material, **DPivOHAC**, and  
203 the chemically synthesized **DPivOHAQ**. The top three spectra in Figure 3d are the  $^1\text{H}$  NMR  
204 spectra from electrosynthesized **DPivOHAQ**, in which the dominating peaks have the same  
205 chemical shifts as those in the spectrum of chemically synthesized **DPivOHAQ**, further suggesting  
206 the desired product was achieved.

207 Slightly different yields of **DPivOHAQ** were obtained when paired with the HER in an  
208 undivided cell or with  $\text{Fe}(\text{CN})_6^{3-}$  reduction or the ORR in a divided cell (Figure S4). The 82.7%  
209 yield when paired with the HER in an undivided cell could be explained by a molecular shuttling  
210 effect; *i.e.*, the electrosynthesized **DPivOHAQ** can first migrate to the cathode where it is reduced,  
211 then diffuse back to the anode for re-oxidation. As a result, double counting of electrons can occur.  
212 When paired with the  $\text{Fe}(\text{CN})_6^{3-}$  reduction half reaction, a yield of 93.0% was obtained. The  
213 incomplete yield is likely due to the consumption and therefore decreased concentration of both  
214 **DPivOHAC** and  $\text{OH}^-$  as the electrosynthesis continues, making further oxidation increasingly  
215 difficult.

216 The use of the ORR half reaction achieved almost 100.0% yield. This exceptional yield may be  
 217 attributed to the as-formed  $\text{OH}^-$  ions on the cathode (ORR) side crossing over to the anolyte and  
 218 compensating for any loss of  $\text{OH}^-$  ions on the anode side. Overall yields in excess of 80.0% for all  
 219 three conditions exceed many conventional reactions and are acceptable for direct flow battery use  
 220 without purification or separation.



221  
 222 **Figure 4. Full cell performance evaluation from Electrosynthesis III and IV.** (a) A  
 223 representative charge–discharge profile with 0.1 M **DPivOHAQ**. Negolyte: 5 mL of 0.1 M  
 224 **DPivOHAQ** pH = ~13.5. Posolyte: 100 mL of 0.1 M potassium ferro-/ferricyanide solution [~0.06  
 225 M  $\text{K}_4\text{Fe}(\text{CN})_6$  and ~0.04 M  $\text{K}_3\text{Fe}(\text{CN})_6$ ] pH = ~13.6. (b) Discharge capacity (C) and coulombic  
 226 efficiency (%) vs. cycle number and time (days). Negolyte: 4.5 mL of 0.1 M **DPivOHAQ**. Posolyte:  
 227 100 mL of 0.1 M ferro-/ferricyanide solution [~0.06 M  $\text{K}_4\text{Fe}(\text{CN})_6$  and ~0.04 M  $\text{K}_3\text{Fe}(\text{CN})_6$ ].  
 228 Current density: 30 mA/cm<sup>2</sup> with potential hold (cutoffs: 0.6 V, 1.2 V) until current decreased to  
 229 2 mA/cm<sup>2</sup>. (c) A representative charge–discharge profile with 0.5 M **DPivOHAQ**. Negolyte: 6  
 230 mL of 0.5 M **DPivOHAQ**. Posolyte: 100 mL of 0.5 M potassium ferro-/ferricyanide solution [~0.3

231 M K<sub>4</sub>Fe(CN)<sub>6</sub> and ~0.2 M K<sub>3</sub>Fe(CN)<sub>6</sub>]. Current density: 100 mA/cm<sup>2</sup> with potential hold (cutoff:  
232 0.4 V, 1.4 V) until current decreased to 2 mA/cm<sup>2</sup>. (d) Polarization curves of the 0.5 M  
233 **DPivOHAQ** at the SOC of 20%, 40%, 60%, 80%, and ~100% respectively. Descriptions of  
234 **Electrosynthesis III and IV** can be found in the Supporting Information.

235  
236 To demonstrate the feasibility of switching from the electrosynthesis mode (when paired with  
237 Fe(CN)<sub>6</sub><sup>3-</sup> reduction) to flow battery mode, we began charge–discharge cycling immediately upon  
238 completion of the electrosynthesis, without performing any purification. Because other research  
239 has reported that quinones and related compounds can decompose in the presence of light,<sup>40-42</sup> we  
240 wrapped the electrolyte reservoirs with aluminum foil to avoid light-induced decomposition during  
241 cell cycling (Figures S13–S15). Figure 4a shows the charge–discharge profile of a single cycle  
242 with an open circuit voltage of ~1.0 V and a capacity of 84.0 coulombs. Given the 93.0% yield  
243 found from the <sup>1</sup>H NMR, the capacity utilization is 93.6%. Long-term cycling was then performed  
244 to determine a temporal capacity fade rate of the full cell. Figure 4b demonstrates the discharge  
245 capacity and coulombic efficiency over 33.2 days and 2271 cycles with a fitted fade rate of  
246 0.014%/day and an average coulombic efficiency of 99.53%. This is consistent with the fade rate  
247 of chemically synthesized **DPivOHAQ**.<sup>38</sup> The extremely low capacity fade rate is attributed to the  
248 chemical stability of the molecular structure. The C–C covalent bond between the anthraquinone  
249 core and the functionalizing chains is more robust in strong base and at elevated temperature than  
250 the C–O bond demonstrated in previous work.<sup>4, 5, 38</sup> Furthermore, the two branched methyl groups  
251 on the carbon connected to the anthraquinone (AQ) core may increase the stability of the  
252 solubilizing chain even when exposed to harsh conditions.<sup>15</sup>

253 To examine the feasibility of this method for potential industry use, we further conducted  
254 electrosynthesis with a higher concentration (0.5 M) of **DPivOHAC** at a higher current density  
255 (100 mA/cm<sup>2</sup>) (See Figure S5). Figure 4c shows that 0.5 M electrosynthesized negolyte can deliver  
256 72.9% of the theoretical capacity. We attribute the discrepancy between the delivered capacity and

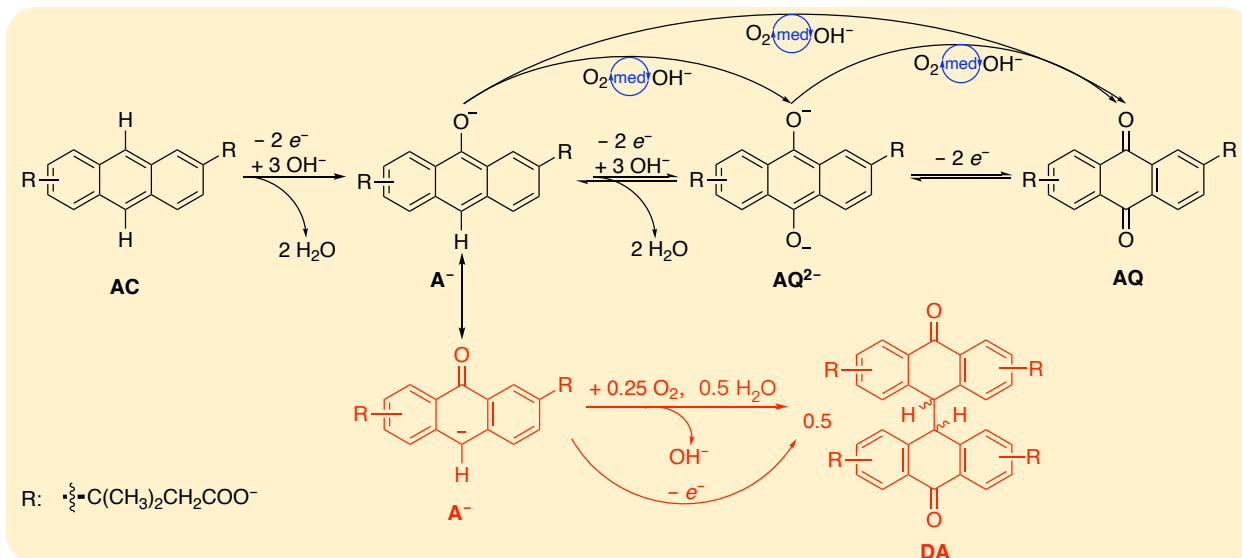
257 the theoretical capacity primarily to incomplete conversion (Figure S6). The capacity utilization is  
258 81.9% if we consider that there is 11.0% unreacted **DPivOHAC(COO<sup>-</sup>)** in the negolyte.  
259 Additionally, the mass transport of active species at 0.5 M concentration may be another issue  
260 limiting the full capacity utilization. The corresponding polarization curve at different states of  
261 charge (SOC) is shown in Figure 4d. The peak power density exceeds 0.2 W/cm<sup>2</sup> when at ~100 %  
262 of SOC.

263 Given the total transfer of six electrons during the electrosynthesis of **DPivOHAC** to  
264 **DPivOHAQ**, the high yields achieved in this work might be surprising. We hypothesize a three-  
265 step successive two-electron transfer mechanism<sup>34, 35</sup>: first, when a potential is applied, anthracene  
266 (**AC**) may react with three OH<sup>-</sup> ions and donate two electrons to produce two water molecules and  
267 the anthrone anion (**A<sup>-</sup>**); second, **A<sup>-</sup>** may further react with another three OH<sup>-</sup> ions and donate  
268 another two electrons to generate two water molecules and the deprotonated anthrahydroquinone  
269 dianion (**AQ<sup>2-</sup>**); third, **AQ<sup>2-</sup>** may further release two electrons to afford the anthraquinone species  
270 (**AQ**). Complete electrochemical conversion in the third step has been well-documented at  
271 negative potentials vs. ferro-/ferricyanide<sup>1, 2, 43</sup> and should therefore be rapid at positive potentials  
272 vs. ferro-/ferricyanide. The reverse reaction of the second step has recently been identified as a  
273 side reaction in ARFBs, and the forward reaction is chemically feasible when exposed to O<sub>2</sub> or  
274 air.<sup>14, 38</sup> Given the high voltage applied to the cell, it is thus plausible that the forward reactions  
275 (**AC** to **A<sup>-</sup>** to **AQ<sup>2-</sup>/AQ**) can electrochemically proceed completely and swiftly.

276 Our group has also previously proposed a side reaction pathway for anthraquinones,<sup>14, 44</sup> where  
277 the anthrone anion (**A<sup>-</sup>**) can be oxidatively dimerized to dianthrone (**DA**) chemically and/or  
278 electrochemically. According to <sup>1</sup>H NMR spectra (Figure 3d) and liquid chromatography–mass  
279 spectrometry (LC–MS) results (Figure S7), neither **DA** nor Kolbe electrolysis-related byproducts<sup>45</sup>

280 were detected (Scheme S1), suggesting that **AC/AQ**-related side reactions can be negligible when  
281 a sufficient  $\text{OH}^-$  concentration is present to prevent dianthrone formation and a sufficiently low  
282 voltage cutoff is chosen to prevent Kolbe electrolysis dimer formation. The major competing side  
283 reaction is the OER, which, along with the reactions of **AC** to  $\text{A}^-$  to  $\text{AQ}^{2-}$ , will consume  $\text{OH}^-$  and  
284 may lead to the formation of **DA** as a result of insufficient  $\text{OH}^-$  ions in the **DPivOHAC** solution  
285 (see **Electrosynthesis V** in the SI). Interestingly, the dianthrones (Scheme S2), detected by  
286 LC-MS (Figure S11), are surprisingly redox-active when a broad voltage window is applied  
287 (Figures S8 and S9 and Scheme S2). On the one hand, the OER can reduce faradaic efficiency; on  
288 the other hand, the generated oxygen can serve as a mediator and chemically oxidize intermediates  
289 (*i.e.*,  $\text{A}^-$ ,  $\text{AQ}^{2-}$ ) to the final **AQ** form, *i.e.*, mediated (indirect) electrochemical oxidation. Because  
290 the entire process involves not only electrochemical oxidations, but also chemical oxidations, it is  
291 more appropriate to call it an electrochemical-chemical oxidation process.<sup>46</sup>

292 In the proposed mechanism, the anthrone derivative is an intermediate in the electrochemical  
293 oxidation. Anthrone formation has been identified as the major side reaction causing capacity fade  
294 in previous work;<sup>14, 38</sup> therefore, it is plausible that lost capacity of anthraquinone flow battery  
295 systems may be recovered and anthraquinone lifetime extended by electrochemically oxidizing  
296 anthrone to redox-active anthraquinone derivatives.



297

298 **Scheme 1. Proposed electrochemical oxidation mechanism.** Three-step successive two-electron  
 299 transfer process from **AC** to **A<sup>-</sup>**, **A<sup>-</sup>** to **AQ<sup>2-</sup>**, and **AQ<sup>2-</sup>** to **AQ**. The generated oxygen from the  
 300 OER side reaction may incur chemical oxidation processes including **A<sup>-</sup>** to **AQ<sup>2-</sup>**, **AQ<sup>2-</sup>** to **AQ**,  
 301 and oxidative dimerization (**A<sup>-</sup>** to **DA**).

302

303 To demonstrate that the electrochemical oxidation can be applied to other anthracene  
 304 derivatives, we performed electrochemical oxidation of 4,4'-(9,10-dihydroanthracene-  
 305 diyl)dibutanoic acid (**DBDHAC**), where the molecular core is 9,10-dihydroanthracene.<sup>38</sup> The <sup>1</sup>H  
 306 NMR results indicate that **DBDHAC** can, like **DPivOHAQ**, be electrochemically oxidized to the  
 307 final anthraquinone (Figure S12), **DBAQ** (4,4'-(9,10-anthraquinone-diyl)dibutanoic acid), which  
 308 has also been shown to be extremely stable.<sup>38</sup>

309 The shared precursor of **DPivOHAQ** and **DBAQ**, anthracene, is abundant in crude petroleum  
 310 and coal tar, and can be synthesized from benzene and benzyl alcohol (Scheme S3).<sup>47</sup> The  
 311 precursor of **DPivOHAQ**, 3,3'-dimethyl acrylic acid, can be industrially produced from malonic  
 312 acid, a food acid; the precursor of **DBAQ**, succinic anhydride, can be industrially hydrogenated  
 313 from maleic anhydride and used as an important intermediate on an industrial scale. Thus, both  
 314 **DPivOHAQ** and **DBAQ** can be readily synthesized from commodity chemicals. Although the  
 315 synthetic cost of **DPivOHAQ** or **DBAQ** should be somewhat higher than that of 2,6-

316 dihydroxyanthraquinone (**DHAQ**) due to more steps and more chemicals involved, the capital cost  
317 of AORFBs that utilize finite-lifetime electrolytes can be viewed as including the total active cost,  
318 which is the sum of the initial cost of redox-active materials and the present value of the future  
319 costs of periodic electrolyte replacement.<sup>13</sup> This can lead to an initial cost—lifetime trade-off in  
320 the choice of electrolytes. Over an extended operational lifetime, the total active cost of  
321 **DPivOHAQ** or **DBAQ** may be less than that of **DHAQ** due to their much longer lifetimes.<sup>14</sup>

322

### 323 Conclusion

324 This work demonstrates a potentially scalable, safe, green, and economical *in situ*  
325 electrosynthetic method for anthraquinone electrolytes in a flow cell without the use of hazardous  
326 oxidants or precious metal catalysts. The as-generated electrolytes, which are extremely stable,  
327 can be immediately used in a redox flow battery without separation or purification. Other low-cost  
328 compounds may also be amenable to this approach, providing a pathway to lower the cost of  
329 electrochemical grid storage systems, thereby accelerating the development of a renewable energy  
330 economy. The technique extends the opportunities for direct aqueous electrosynthesis to replace  
331 thermochemical synthesis of value-added organics.

332

### Supplementary Information

333 Supplementary Information can be found with this article online at

334

### Acknowledgments

335 This research was supported by U.S. DOE award DE-AC05-76RL01830 through PNNL  
336 subcontract 428977, Innovation Fund Denmark via the Grand Solutions project "ORBATS" file  
337 no. 7046-00018B, and NSF grant CBET-1914543. D.A.P. acknowledges funding support from the  
338 NSF Graduate Research Fellowship Program, no. DGE1144152 and DGE1745303.

339

### Declaration of Interests

340 Harvard University has filed a patent application on the materials and the electrosynthetic methods  
341 described in this paper.

342

## REFERENCES

344 1. B. Huskinson, M. P. Marshak, C. Suh, S. Er, M. R. Gerhardt, C. J. Galvin, X. Chen, A. Aspuru-  
345 Guzik, R. G. Gordon and M. J. Aziz, *Nature*, 2014, **505**, 195–198.

346 2. K. Lin, Q. Chen, M. R. Gerhardt, L. Tong, S. B. Kim, L. Eisenach, A. W. Valle, D. Hardee, R. G.  
347 Gordon, M. J. Aziz and M. P. Marshak, *Science*, 2015, **349**, 1529–1532.

348 3. M. Moore, R. Counce, J. Watson and T. Zawodzinski, *Journal of Advanced Chemical  
349 Engineering*, 2015, **5**, doi:10.4172/2090-4568.1000140.

350 4. D. G. Kwabi, K. Lin, Y. Ji, E. F. Kerr, M.-A. Goulet, D. De Porcellinis, D. P. Tabor, D. A.  
351 Pollack, A. Aspuru-Guzik, R. G. Gordon and M. J. Aziz, *Joule*, 2018, **2**, 1894–1906.

352 5. Y. Ji, M.-A. Goulet, D. A. Pollack, D. G. Kwabi, S. Jin, D. De Porcellinis, E. F. Kerr, R. G.  
353 Gordon and M. J. Aziz, *Adv. Energy Mater.*, 2019, **9**, 1900039.

354 6. A. Hollas, X. Wei, V. Murugesan, Z. Nie, B. Li, D. Reed, J. Liu, V. Sprengle and W. Wang,  
355 *Nature Energy*, 2018, **3**, 508–514.

356 7. C. Wang, X. Li, B. Yu, Y. Wang, Z. Yang, H. Wang, H. Lin, J. Ma, G. Li and Z. Jin, *ACS Energy  
357 Letters*, 2020, **5**, 411–417.

358 8. J. D. Hofmann, F. L. Pfanschilling, N. Krawczyk, P. Geigle, L. Hong, S. Schmalisch, H. A.  
359 Wegner, D. Mollenhauer, J. Janek and D. Schröder, *Chemistry of Materials*, 2018, **30**, 762–774.

360 9. D. G. Kwabi, Y. Ji and M. J. Aziz, *Chem. Rev.*, 2020, **120**, doi.org/10.1021/acs.chemrev.9b00599.

361 10. Z. Yang, L. Tong, D. P. Tabor, E. S. Beh, M.-A. Goulet, D. De Porcellinis, A. Aspuru-Guzik, R.  
362 G. Gordon and M. J. Aziz, *Adv. Energy Mater.*, 2018, **8**, 1702056.

363 11. V. Dieterich, J. D. Milshtein, J. L. Barton, T. J. Carney, R. M. Darling, F. R. Brushett,  
364 *Translational Materials Research*, 2018, **5**, 034001.

365 12. S. Jin, E. M. Fell, L. Vina-Lopez, Y. Jing, P. W. Michalak, R. G. Gordon and M. J. Aziz, *Adv.  
366 Energy Mater.*, 2020, **10**, doi.org/10.1002/aenm.202000100.

367 13. F. R. Brushett, M. J. Aziz and K. E. Rodby, *ACS Energy Letters*, 2020, **5**, 879–884.

368 14. M.-A. Goulet, L. Tong, D. A. Pollack, D. P. Tabor, S. A. Odom, A. Aspuru-Guzik, E. E. Kwan,  
369 R. G. Gordon and M. J. Aziz, *J. Am. Chem. Soc.*, 2019, **141**, 8014–8019.

370 15. P. Anastas, N. Eghbali, *Chem. Soc. Rev.*, 2010, **39**, 301–312.

371 16. D. S. P. Cardoso, B. Šljukić, D. M. F. Santos, C. A. C. Sequeira, *Organic Process Research &  
372 Development*, 2017, **21**, 1213–1226.

373 17. M. Yan, Y. Kawamata, P. S. Baran, *Chem. Rev.*, 2017, **117**, 13230–13319.

374 18. B. K. Peters, K. X. Rodriguez, S. H. Reisberg, S. B. Beil, D. P. Hickey, Y. Kawamata, M.  
375 Collins, J. Starr, L. Chen, S. Udyavara, K. Klunder, T. J. Gorey, S. L. Anderson, M. Neurock, S.  
376 D. Minteer and P. S. Baran, *Science*, 2019, **363**, 838–845.

377 19. E. J. Horn, B. R. Rosen, Y. Chen, J. Tang, K. Chen, M. D. Eastgate, P. S. Baran, *Nature*, 2016,  
378 **533**, 77–81.

379 20. A. Badalyan, S. S. Stahl, *Nature*, 2016, **535**, 406–410.

380 21. G. G. Botte, *The Electrochemical Society Interface*, 2014, **23**, 49–55.

381 22. P. M. Bersier, L. Carlsson and J. Bersier, *Topics in Current Chemistry*, 1994, **170**, 116–136.

382 23. C. Xia, Y. Xia, P. Zhu, L. Fan and H. Wang, *Science*, 2019, **366**, 226–231.

383 24. M. Granda, C. Blanco, P. Alvarez, J. W. Patrick and R. Menendez, *Chem. Rev.*, 2014, **114**, 1608–  
384 1636.

385 25. R. S. Tipson, in *National Bureau of Standards Monograph 87*, 1965, 1–49.

386 26. R. P. Kreh, R. M. Spotnitz and J. T. Lundquist, *J. Org. Chem.*, 1989, **54**, 1531–1535.

387 27. E. Oppermann, *US Pat.*, US823,435A, 1906.

388 28. E. Steckhan, in *Ullmann's Encyclopedia of Industrial Chemistry*, Wiley-VCH Verlag GmbH &  
389 Co. KGaA, Weinheim, 2011, **12**, DOI: 10.1002/14356007.009\_004.

390 29. R. M. Spotnitz, R. P. Kreh, J. T. Lundquist and P. J. Press, *Journal of Applied Electrochemistry*,  
391 1990, **20**, 209–215.

392 30. R. P. Kreh, R. M. Spotnitz and J. T. Lundquist, *Tetrahedron Letters*, 1987, **28**, 1067–1068.

393 31. E. J. Majeski, J. D. Stuart and W. E. Ohnesorge, *J. Am. Chem. Soc.*, 1968, **90**, 633–636.

394 32. L. R. Faulkner, A. J. Bard, *J. Am. Chem. Soc.*, 1968, **90**, 6284–6290.

395 33. C. Amatore and A. R. Brown, *J. Am. Chem. Soc.*, 1996, **118**, 1482–1486.

396 34. O. Tovide, N. Jahed, C. E. Sunday, K. Pokpas, R. F. Ajayi, H. R. Makelane, K. M. Molapo, S. V.  
397 John, P. G. Baker and E. I. Iwuoha, *Sensors and Actuators B: Chemical*, 2014, **205**, 184–192.

398 35. C. A. Paddon, C. E. Banks, I. G. Davies and R. G. Compton, *Ultrason. Sonochem.*, 2006, **13**,  
399 126–132.

400 36. V. D. Parker, *Acta Chemica Scandinavica*, 1970, **24**, 2757–2767.

401 37. T. Noel, Y. Cao and G. Laudadio, *Acc. Chem. Res.*, 2019, **52**, 2858–2869.

402 38. M. Wu, Y. Jing, A. A. Wong, E. M. Fell, S. Jin, Z. Tang, R. G. Gordon and M. J. Aziz, *Chem*,  
403 2020, **6**, 1432–1442.

404 39. R. W. Zurilla, R. K. Sen and E. Yeager, *J. Electrochem. Soc.*, 1978, **125**, 1103–1109.

405 40. G. Maier, L. H. Franz, H.-G. Hartan, K. Lanz and H. P. Reisenauer, *Chemische Berichte*, 1985,  
406 **118**, 3196–3204.

407 41. S. A. Carlson and D. M. Hercules, *Analytical Chemistry*, 1973, **45**, 1794–1799.

408 42. B. E. Hulme, E. J. Land and G. O. Phillips, *J. Chem. Soc. Faraday Trans. 1*, 1972, **68**, 1992–  
409 2002.

410 43. M. Quan, D. Sanchez, M. F. Wasylkiw and D. K. Smith, *J. Am. Chem. Soc.*, 2007, **129**, 12847–  
411 12856.

412 44. S. Jin, Y. Jing, D. G. Kwabi, Y. Ji, L. Tong, D. De Porcellinis, M. A. Goulet, D. A. Pollack, R. G.  
413 Gordon and M. J. Aziz, *ACS Energy Letters*, 2019, **4**, 1342–1348.

414 45. H.-J. Schäfer, *Topics in Current Chemistry*, 1990, **152**, 91–151.

415 46. C. Costentin and J.-M. Savéant, *Proc. Natl. Acad. Sci. U S A*, 2019, **116**, 11147–11152.

416 47. H. E. Ugnade and E. W. Crandall, *J. Am. Chem. Soc.*, 1949, **71**, 3009–3010.

417

## Supplementary Information

## ***In situ* Electrosynthesis of Anthraquinone Electrolytes in Aqueous Flow Batteries**

Yan Jing,<sup>1§</sup> Min Wu,<sup>2§</sup> Andrew A. Wong,<sup>2</sup> Eric M. Fell,<sup>2</sup> Shijian Jin,<sup>2</sup> Daniel A. Pollack,<sup>3</sup> Emily F. Kerr,<sup>1</sup> Roy G. Gordon,<sup>\*,1,2</sup> Michael J. Aziz<sup>\*,2</sup>

<sup>1</sup> Department of Chemistry and Chemical Biology, Harvard University, Cambridge, Massachusetts 02138, United States

<sup>2</sup> John A. Paulson School of Engineering and Applied Sciences, Harvard University, Cambridge, Massachusetts 02138, United States

<sup>3</sup> Department of Physics, Harvard University, Cambridge, Massachusetts 02138, United States

§ These authors contributed equally to this work.

\* Correspondence: [gordon@chemistry.harvard.edu](mailto:gordon@chemistry.harvard.edu); [maziz@harvard.edu](mailto:maziz@harvard.edu)

## Table of Contents

15	<b>General information for synthesis and characterization .....</b>	<b>3</b>
16	<b>Electrochemical characterization .....</b>	<b>3</b>
17	<b>Brief description of electrosynthesis .....</b>	<b>3</b>
18	<b>Figure S1. <math>^1\text{H}</math> NMR spectra of commercial and synthesized 9,10-dihydroanthracene (DHAC) in</b>	
19	<b>DMSO-<math>d_6</math>.....</b>	<b>4</b>
20	<b>Figure S2. <math>^1\text{H}</math> NMR spectra of 2,7-, 2,6-DPivOHAC isomers and their mixture (aromatic region)</b>	
21	<b>in DMSO-<math>d_6</math>.....</b>	<b>5</b>
22	<b>Figure S3. Photos of undivided cell (a) and divided cell (b).....</b>	<b>5</b>
23	<b>Figure S4. Schematics of (a) undivided cell against the HER and divided cells against (b) the</b>	
24	<b>ORR and (c) ferricyanide to ferrocyanide, respectively. .....</b>	<b>6</b>
25	<b>Electrosynthesis I. Electrochemical synthesis of DPivOHAQ(<math>\text{COO}^-</math>) in an undivided cell at 0.1 M</b>	
26	<b>concentration, against the hydrogen evolution reaction (HER).....</b>	<b>7</b>
27	<b>Electrosynthesis II. Electrochemical synthesis of DPivOHAQ(<math>\text{COO}^-</math>) in a divided cell at 0.1 M</b>	
28	<b>concentration, against the oxygen reduction reaction (ORR).....</b>	<b>8</b>
29	<b>Electrosynthesis III. Electrochemical synthesis of DPivOHAQ(<math>\text{COO}^-</math>) in a divided cell at 0.1 M</b>	
30	<b>concentration, against the reduction of ferricyanide. .....</b>	<b>8</b>
31	<b>Electrosynthesis IV. Electrochemical synthesis of DPivOHAQ(<math>\text{COO}^-</math>) in a divided cell at 0.5 M</b>	
32	<b>concentration with excess hydroxide, against the reduction of ferricyanide. .....</b>	<b>9</b>
33	<b>Figure S5. The electrochemical oxidation of 0.5 M DPivOHAC(<math>\text{COO}^-</math>) (Electrosynthesis IV)....</b>	<b>10</b>

34	<b>Figure S6.</b> $^1\text{H}$ NMR spectrum of DPivOHAQ in $\text{DMSO}-d_6$ synthesized via the procedure described in Electrosynthesis IV. From the aromatic peak integrations, we found that 89.0% DPivOHAQ was generated (when the two set of peaks at chemical shifts of 7.95 and 8.10 ppm were integrated), 11.0% DPivOHAC was remaining.....	11
38	<b>Figure S7.</b> Mass spectra of partially electrosynthesized DPivOHAQ (from Electrosynthesis IV) measured by liquid chromatography–mass spectrometry (LC–MS). .....	12
40	<b>Scheme S1.</b> Kolbe electrolysis. ....	13
41	<b>Electrosynthesis V.</b> Electrochemical synthesis of DPivOHAQ( $\text{COO}^-$ ) in a divided cell at 0.5 M concentration with a stoichiometric quantity of hydroxide, against the reduction of ferricyanide. ....	13
44	<b>Formation of dianthrone during electrosynthesis</b> .....	14
45	<b>Figure S8.</b> Cell performance of 0.5 M electrosynthesized DPivOHAQ when a stoichiometric quantity of hydroxide was added into the DPivOHAC( $\text{COO}^-$ ) solution (Electrosynthesis V).....	14
47	<b>Figure S9.</b> Voltage profiles of 0.5 M electrosynthesized DPivOHAQ when a stoichiometric quantity of hydroxide was added into the DPivOHAC solution (Electrosynthesis V) with different lower voltage cutoffs [(a) 0.6, (b) 0.2, (c) 0.6, and (d) 0.7 V].....	15
50	<b>Figure S10.</b> $^1\text{H}$ NMR spectrum of cycled 0.5 M electrosynthesized DPivOHAQ when a stoichiometric quantity of hydroxide was added into the DPivOHAC( $\text{COO}^-$ ) solution (Electrosynthesis V). .....	16
53	<b>Figure S11.</b> LC–MS results of cycled 0.5 M electrosynthesized DPivOHAQ when a stoichiometric quantity of hydroxide was added into the DPivOHAC solution (Electrosynthesis V). .....	17
55	<b>Electrosynthesis VI.</b> Electrochemical synthesis of DBAQ( $\text{COO}^-$ ) in an undivided electrolytic cell at 0.1 M concentration, against the HER.....	18
57	<b>Figure S12.</b> $^1\text{H}$ NMR spectra of DBDHAC (bottom), chemically synthesized DBAQ (top), and electrochemically synthesized DBAQ in an undivided cell after varying extents of reaction. ....	19
59	<b>Light sensitivity experiments</b> .....	19
60	<b>Figure S13.</b> Samples of (a) DPivOHAQ (0.1 M, pH 12) stored for 1 week in the absence of light (– $\text{h}\nu$ ) and under a 500 W lamp (+ $\text{h}\nu$ ) and of (b) DBAQ (0.1 M, pH 12) stored for 1 week in the absence of light (– $\text{h}\nu$ ) and under a 500 W lamp (+ $\text{h}\nu$ ). Differences in color were observed between the two samples of each compound. The formation of a film was also observed in the DPivOHAQ sample exposed to light. ....	20
65	<b>Figure S14.</b> $^1\text{H}$ NMR spectra of samples of DPivOHAQ (0.1 M, pH 12) stored for 1 week in the absence of light (– $\text{h}\nu$ ) and under a 500 W lamp (+ $\text{h}\nu$ ), each diluted (1:5.5) in pH 14 $\text{D}_2\text{O}$ (1 M KOD) containing a 9 mM $\text{NaCH}_3\text{SO}_3$ internal standard ( $\delta$ 2.6 ppm).....	21
68	<b>Figure S15.</b> $^1\text{H}$ NMR spectra of samples of DBAQ (0.1 M, pH 12) stored for 1 week in the absence of light (– $\text{h}\nu$ ) and under a 500 W lamp (+ $\text{h}\nu$ ), each diluted (1:5) in pH 12 $\text{D}_2\text{O}$ or in $\text{DMSO}-d_6$ . .....	22
70	<b>Complete synthesis</b> .....	22

71        **Scheme S3. Complete synthetic routes, conditions, and yields of DPivOHAQ and DBAQ when**  
72        **commercially available commodity chemicals are used as starting materials. .... 23**

73        **Figure S16.  $^1\text{H}$  NMR spectra of commercial and synthesized anthracene (AC) in  $\text{DMSO-}d_6$ . The**  
74        **peak at 7.37 ppm in the synthesized AC spectrum is from benzene. .... 23**

75        **General information for synthesis and characterization**

76        All reagents were purchased from Sigma-Aldrich or Alfa Aesar and used as received unless  
77        otherwise stated. All reactions sensitive to moisture or oxygen were carried out in oven-dried or  
78        flame-dried and nitrogen-charged glassware. All anhydrous solvents were saturated with argon  
79        and passed through a column of activated alumina immediately prior to use.

80         $^1\text{H}$  NMR spectra were recorded on Varian INOVA 500 spectrometers at 500 MHz. NMR spectra  
81        were recorded in solutions of deuterated dimethyl sulfoxide ( $\text{DMSO-}d_6$ ) with the residual dimethyl  
82        sulfoxide ( $\delta$  2.25 ppm for  $^1\text{H}$  NMR), or deuterated water ( $\text{D}_2\text{O}$ ) with the residual  $\text{H}_2\text{O}$  ( $\delta$  4.79 ppm  
83        for  $^1\text{H}$  NMR).

84        LC-MS was conducted on a Bruker microTOF-Q II mass spectrometer. The sample was diluted  
85        by water/acetonitrile (V/V = 1:1) to the desired concentration ( $\sim 20\mu\text{M}$ ) before LC-MS  
86        measurements.

87        **Electrochemical characterization**

88        *Cyclic voltammetry measurements*

89        Glassy carbon was used as the working electrode for all three-electrode CV tests with a 5 mm  
90        diameter glassy carbon working electrode, an Ag/AgCl reference electrode (BASi, pre-soaked in  
91        3 M NaCl solution), and a graphite counter electrode.

92        All electrochemical oxidation and flow cell cycling was conducted with Biologic equipment and  
93        corresponding software.

94        *Flow cell setup*

95        Flow battery experiments were constructed with cell hardware from Fuel Cell Tech (Albuquerque,  
96        NM) assembled into a zero-gap flow cell configuration. Pyrosealed POCO graphite flow plates  
97        with serpentine flow patterns were used for both electrodes. Each electrode comprised a 5  $\text{cm}^2$   
98        geometric surface area covered by a piece of AvCarb HCBA woven carbon fiber. The membrane  
99        is pre-soaked (1 M KOH for 24 hours) Nafion 212.

100        **Brief description of electrosynthesis**

101        *Undivided electrolytic cell setup*

102        Working electrode: carbon felt, where **DPivOHAC(COO $^-$ )** was oxidized to **DPivOHAQ(COO $^-$ )**;  
103        counter electrode: carbon rod, where water was reduced to hydrogen gas.

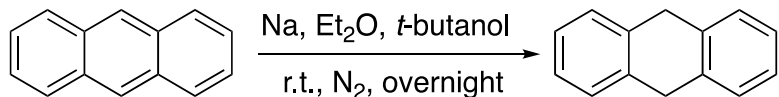
104        *Divided electrolytic cell setup vs. the ORR*

105        Anode: Commercial AvCarb HCBA (woven carbon cloth), where **DPivOHAC(COO $^-$ )** was  
106        oxidized to **DPivOHAQ(COO $^-$ )**; cathode: platinum coated carbon paper (SGL 39AA), where  
107        humidified air/oxygen was reduced to hydroxide.

116 *Divided electrolytic cell setup vs. the reduction of ferricyanide*

117 Anode: AvCarb HCBA (woven carbon cloth), where **DPivOHAC(COO<sup>-</sup>)** was oxidized to  
118 **DPivOHAQ(COO<sup>-</sup>)**; cathode: AvCarb HCBA (woven carbon cloth), where potassium  
119 ferricyanide was reduced to potassium ferrocyanide.

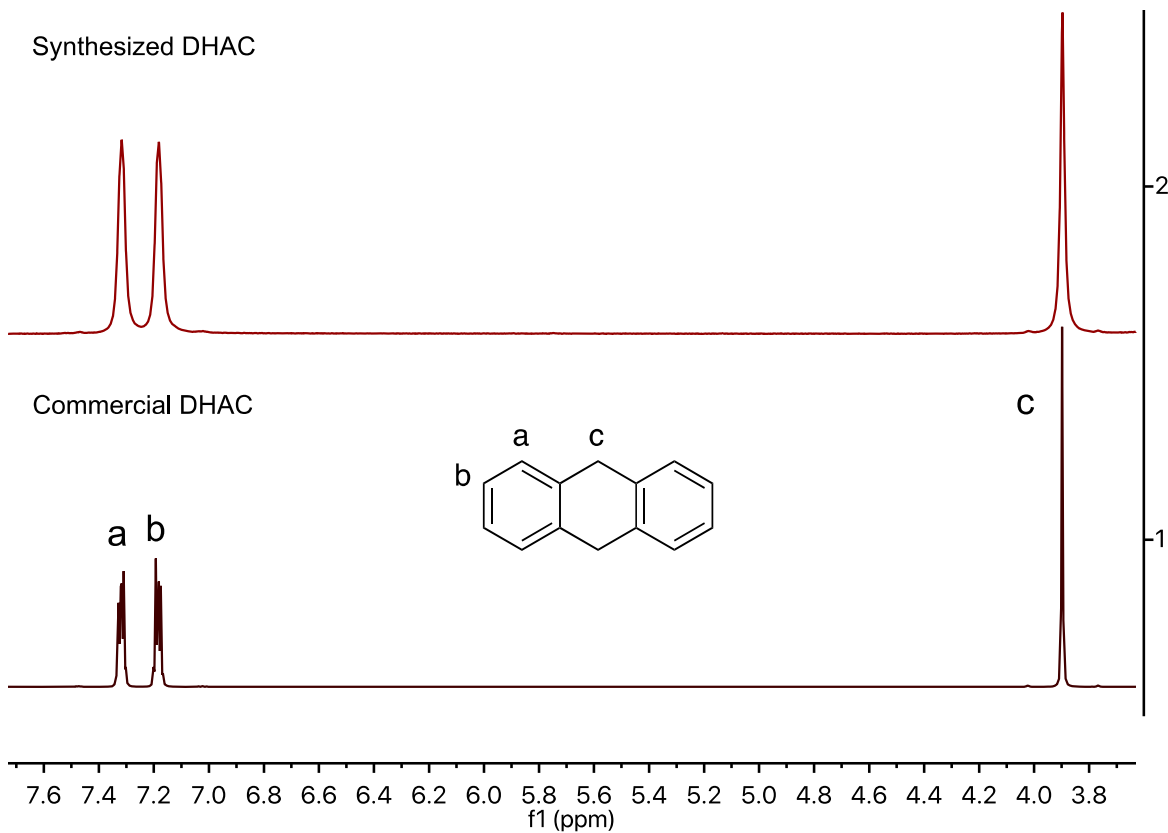
120



AC

DHAC

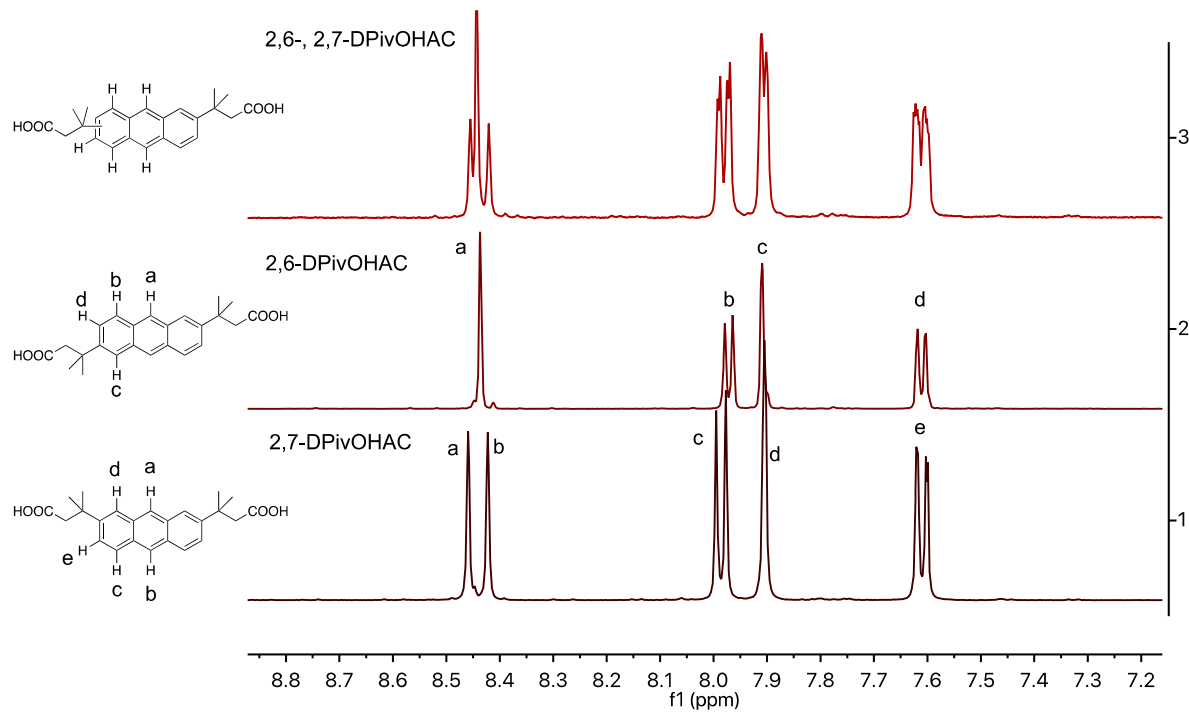
Synthesized DHAC



121

122 **Figure S1.** <sup>1</sup>H NMR spectra of commercial and synthesized 9,10-dihydroanthracene (**DHAC**) in  
123 *DMSO-d*<sub>6</sub>.

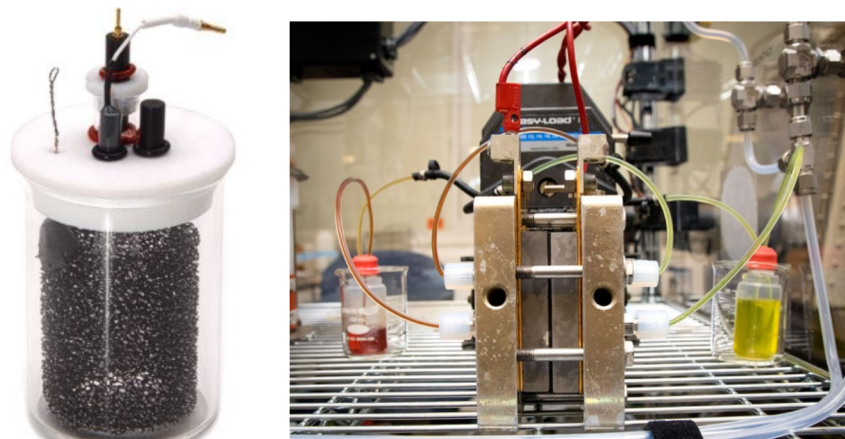
124



125  
126  
127  
128

**Figure S2.**  $^1\text{H}$  NMR spectra of 2,7-, 2,6-DPivOHAC isomers and their mixture (aromatic region) in  $\text{DMSO}-d_6$ .

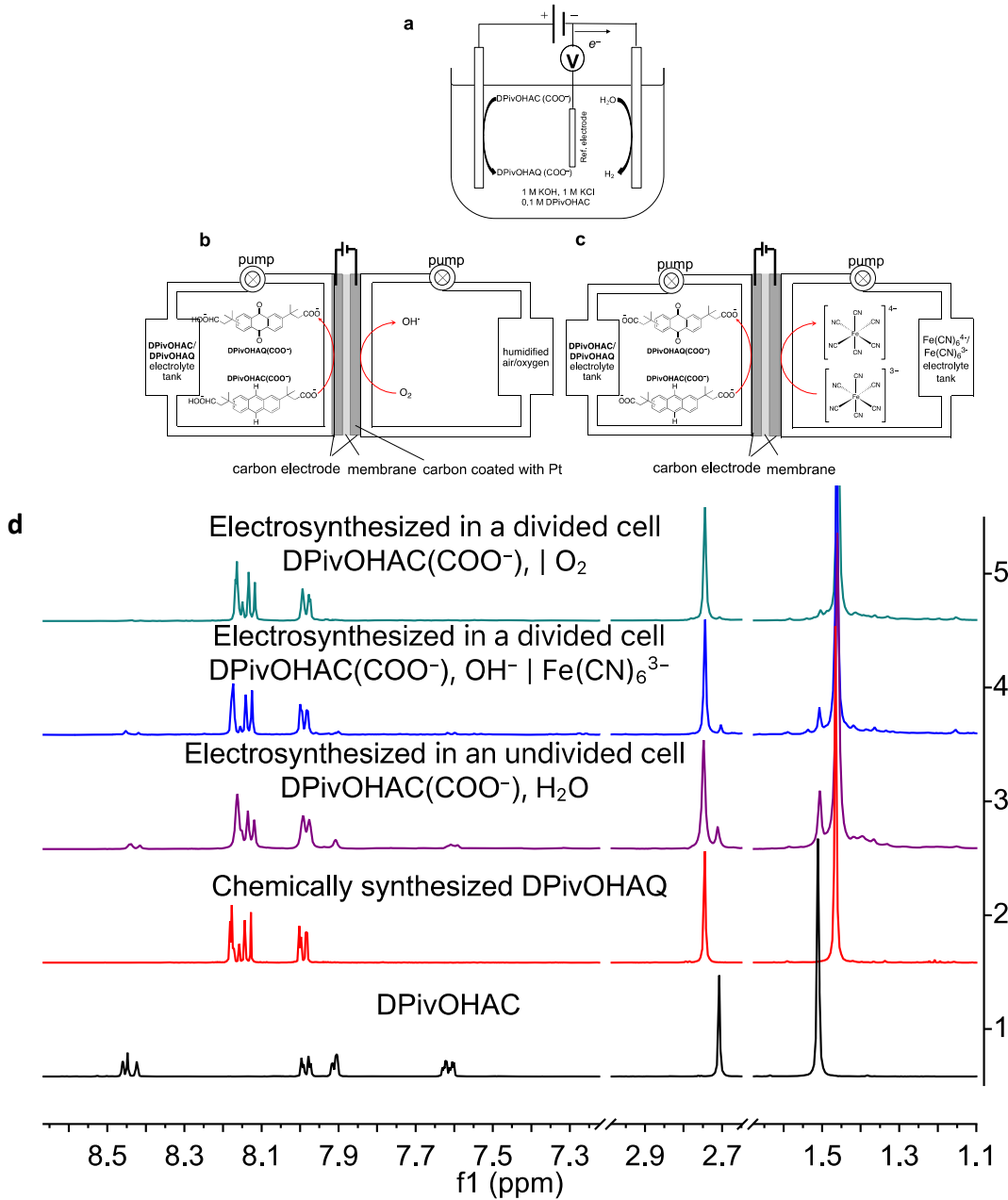
**a** Undivided cell      **b** Divided cell



129  
130  
131

**Figure S3.** Photos of undivided cell (a) and divided cell (b).

132



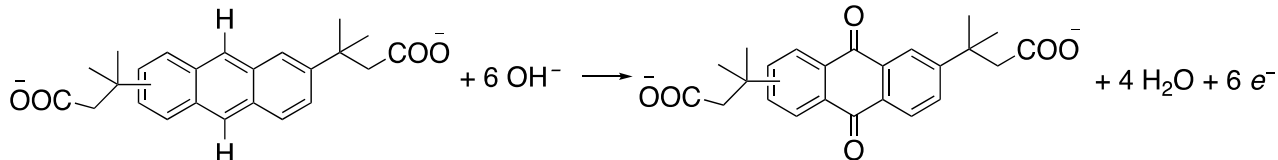
133

134 **Figure S4.** Schematics of (a) undivided cell against the HER and divided cells against (b) the ORR  
 135 and (c) ferricyanide to ferrocyanide, respectively. (d) <sup>1</sup>H NMR spectra of (bottom to top):  
 136 chemically synthesized **DPivOHAC** (black); chemically synthesized **DPivOHQA** (red);  
 137 electrosynthesized **DPivOHAQ** in an undivided cell (purple), 17.3% of **DPivOHAC** remained  
 138 unreacted according to the integration, yield: 82.7%; electro-synthesized **DPivOHAQ** in a divided  
 139 cell against Fe(CN)<sub>6</sub><sup>3-</sup> (blue), 7.0% of **DPivOHAC** remained unreacted according to the  
 140 integration, yield: 93.0%; electrosynthesized **DPivOHAQ** in a divided cell against O<sub>2</sub> (green), 0 %  
 141 of **DPivOHAC** remained unreacted according to the integration, yield: 100%. The deuterated  
 142 solvent is DMSO-*d*<sub>6</sub>, and the solvent peaks (DMSO and H<sub>2</sub>O) were removed to better display the  
 143 peaks of interest. The electrosynthetic details are described under the headings **Electrosynthesis**  
 144 **I, II, and III**.

145



184 **Electrosynthesis II.** Electrochemical synthesis of **DPivOHAQ(COO<sup>-</sup>)** in a divided cell at 0.1 M  
185 concentration, against the oxygen reduction reaction (ORR).  
186



189  
190 In a flow cell setup (divided electrolytic cell), where unbaked AvCarb HCBA was used on the  
191 anode side, the carbon paper was used on the cathode side with coated platinum particles to  
192 catalyze the ORR; Nafion® 212 was used as membrane. The high-frequency area specific  
193 resistance (HF-ASR) was maintained in the range of 1.48–1.54  $\Omega \text{ cm}^2$  before and after  
194 electrosynthesis.

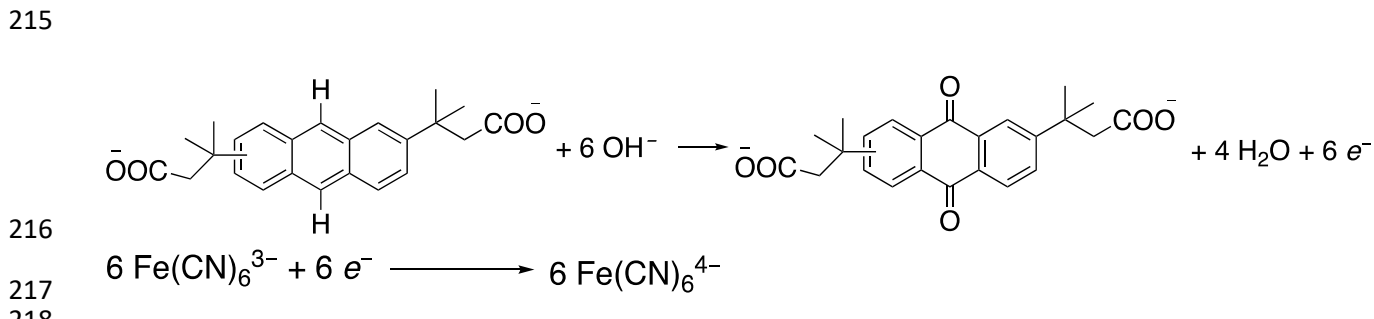
195  
196 Anolyte preparation: 0.378 g **DPivOHAC**, 0.745 g KCl, and 0.561 g KOH were dissolved in  
197 deionized water to obtain a 10 mL solution containing 0.1 M **DPivOHAC**, 1.0 M KCl, and 1.0 M  
198 KOH.

199  
200 Catholyte preparation: humidified oxygen or air was pumped into the flow cell to participate in  
201 the electrochemical reaction.

202  
203 Electrochemical oxidation of **DPivOHAC(COO<sup>-</sup>)**: a constant voltage (1.8 V) was applied to the  
204 divided electrolytic cell until the current decreased to 2 mA/cm<sup>2</sup>. The number of extracted electrons  
205 was ~1.2 times higher than the theoretical value.

206  
207 Characterization of anolyte: an aliquot (~250  $\mu\text{L}$ ) was transferred from the as-prepared anolyte to  
208 an Eppendorf® tube (capacity: 1.5 mL) and acidified by concentrated HCl to obtain **DPivOHAQ**  
209 precipitate. The final **DPivOHAQ** precipitate was re-dissolved in DMSO-*d*<sub>6</sub> for <sup>1</sup>H NMR  
210 measurement. According to the integration of the <sup>1</sup>H NMR spectrum (Figure 3d), the yield is 100%.  
211 The faradaic efficiency (%) = [yield (%) / 1.2] = 83.3%.

212  
213 **Electrosynthesis III.** Electrochemical synthesis of **DPivOHAQ(COO<sup>-</sup>)** in a divided cell at 0.1 M  
214 concentration, against the reduction of ferricyanide.



219 In a flow cell setup (divided electrolytic cell), unbaked AvCarb HCBA (woven carbon cloth) was  
220 used as electrodes for both sides; Nafion® 212 was used as the membrane. The high-frequency  
221 area specific resistance (HF-ASR) was maintained at ~1.12  $\Omega$  cm<sup>2</sup> before and after  
222 electrosynthesis.

223  
224 Anolyte preparation: 0.378 g **DPivOHAC**, 0.745 g KCl, and 0.561 g KOH were dissolved in  
225 deionized water to obtain a 10 mL solution containing 0.1 M **DPivOHAC**, 1.0 M KCl, and 1.0 M  
226 KOH.

227  
228 Catholyte preparation: 3.292 g K<sub>3</sub>Fe(CN)<sub>6</sub>, 7.445 g KCl, and 2.805 g KOH were dissolved in  
229 deionized water to obtain a 100 mL solution containing 0.1 M K<sub>3</sub>Fe(CN)<sub>6</sub>, 1.0 M KCl, and 0.5 M  
230 KOH.

231  
232 The reason for which 0.5 M KOH was added to the catholyte is to counterbalance the added OH<sup>-</sup> in  
233 the anolyte, which is required for the electrosynthesis, thereby suppressing the loss of OH<sup>-</sup> from  
234 the anolyte to the catholyte due to crossover.

235  
236 Electrochemical oxidation of **DPivOHAC(COO<sup>-</sup>)**: a constant current density (20 mA/cm<sup>2</sup>) was  
237 applied to the divided cell for at most 1.5 hours with a 1.2 V voltage cutoff; when either time or  
238 voltage reached the limit, the potential was held (1.2 V vs. ferro-/ferricyanide) until the current  
239 decreased to 2 mA/cm<sup>2</sup>. The number of extracted electrons was ~1.2 times higher than the  
240 theoretical value.

241  
242 Characterization of anolyte: an aliquot (~250  $\mu$ L) was transferred from the as-prepared anolyte to  
243 an Eppendorf® tube (capacity: 1.5 mL) and acidified by a drop of concentrated HCl to obtain  
244 **DPivOHAQ** precipitate. The final **DPivOHAQ** precipitate was re-dissolved in DMSO-*d*<sub>6</sub> for <sup>1</sup>H  
245 NMR measurement. According to the integration of the <sup>1</sup>H NMR spectrum (Figure 3d), the yield  
246 is 93.0%. The faradaic efficiency (%) = [yield (%) / 1.2] = 77.5%.

247  
248 Because a few aliquots were transferred and the volume of as-prepared **DPivOHAQ** changed, 5  
249 mL of the **DPivOHAQ** solution was used as the negolyte and 100 mL of the ferro-/ferricyanide  
250 solution [~0.06 M K<sub>4</sub>Fe(CN)<sub>6</sub> and ~0.04 M K<sub>3</sub>Fe(CN)<sub>6</sub>] generated from **Electrosynthesis III** was  
251 used as the posolyte for charge-discharge cycling. Due to leakage, 4.5 mL of **DPivOHAQ**  
252 remained for subsequent cycling.

253  
254 **Electrosynthesis IV.** Electrochemical synthesis of **DPivOHAQ(COO<sup>-</sup>)** in a divided cell at 0.5 M  
255 concentration with excess hydroxide, against the reduction of ferricyanide.

256  
257 In a flow cell setup (divided electrolytic cell), unbaked AvCarb HCBA (woven carbon cloth) was  
258 used as electrodes for both sides; Nafion® 212 was used as the membrane. The high-frequency  
259 area specific resistance (HF-ASR) was maintained at ~1.1  $\Omega$  cm<sup>2</sup> before and after electrosynthesis.

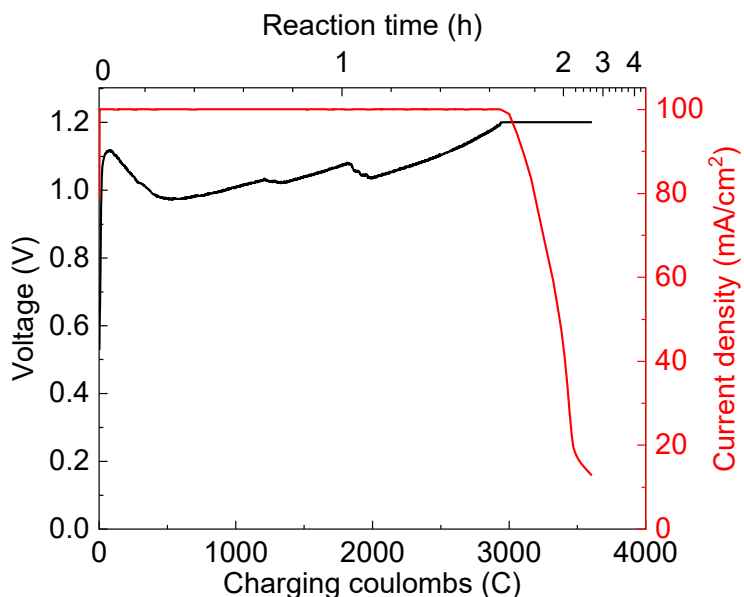
260  
261 Anolyte preparation: 1.89 g **DPivOHAC**, 0.745 g KCl, and 0.567 g KOH were dissolved in  
262 deionized water to obtain a 10 mL solution containing 0.5 M **DPivOHAC**, 1.0 M KCl, and 1.0 M  
263 KOH. Although the **DPivOHAC** electrochemical oxidation requires OH<sup>-</sup> ions, we observed that

264 0.5 M **DPivOHAC** tends to crash out of solution when the concentration of KOH exceeds 1.5 M.  
265 To circumvent this precipitation issue, we added 1.5 times the required amount of KOH pellets  
266 (2.52 g) (*i.e.*, 1.5 times 6 equivalents relative to **DPivOHAC**) into the anolyte over the course of  
267 constant current charging. According to the Nernst equation, the cell voltage is a function of  $[\text{OH}^-]$ ;  
268 thus, the voltage fluctuation reflects the addition of KOH in Figure S5.

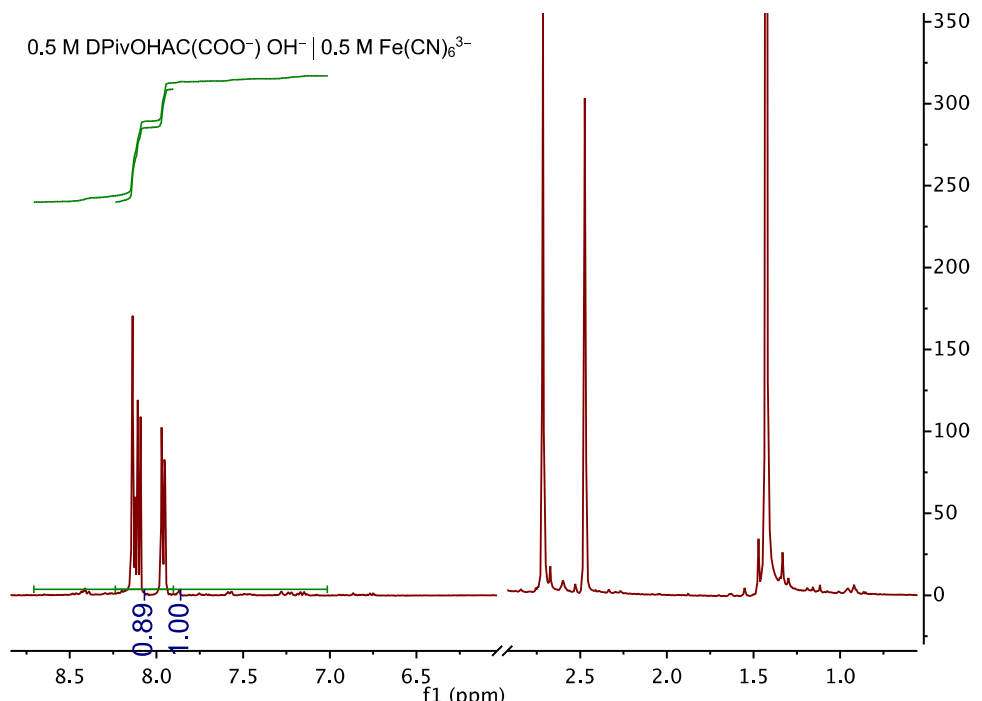
269  
270 Catholyte preparation: 16.46 g  $\text{K}_3\text{Fe}(\text{CN})_6$ , 7.445 g KCl, and 2.805 g KOH were dissolved in  
271 deionized water to obtain a 100 mL solution containing 0.5 M  $\text{K}_3\text{Fe}(\text{CN})_6$ , 1.0 M KCl, and 0.5 M  
272 KOH.

273  
274 Electrochemical oxidation of **DPivOHAC(COO<sup>-</sup>)**: a constant current density (100 mA/cm<sup>2</sup>) was  
275 applied to the divided cell for at most 1.7 hours with a 1.2 V voltage cutoff; when either time or  
276 voltage reached the limit, the potential was held (1.2 V vs. ferro-/ferricyanide) until the current  
277 decreased to 12 mA/cm<sup>2</sup>. The number of extracted electrons was ~1.2 times higher than the  
278 theoretical value.

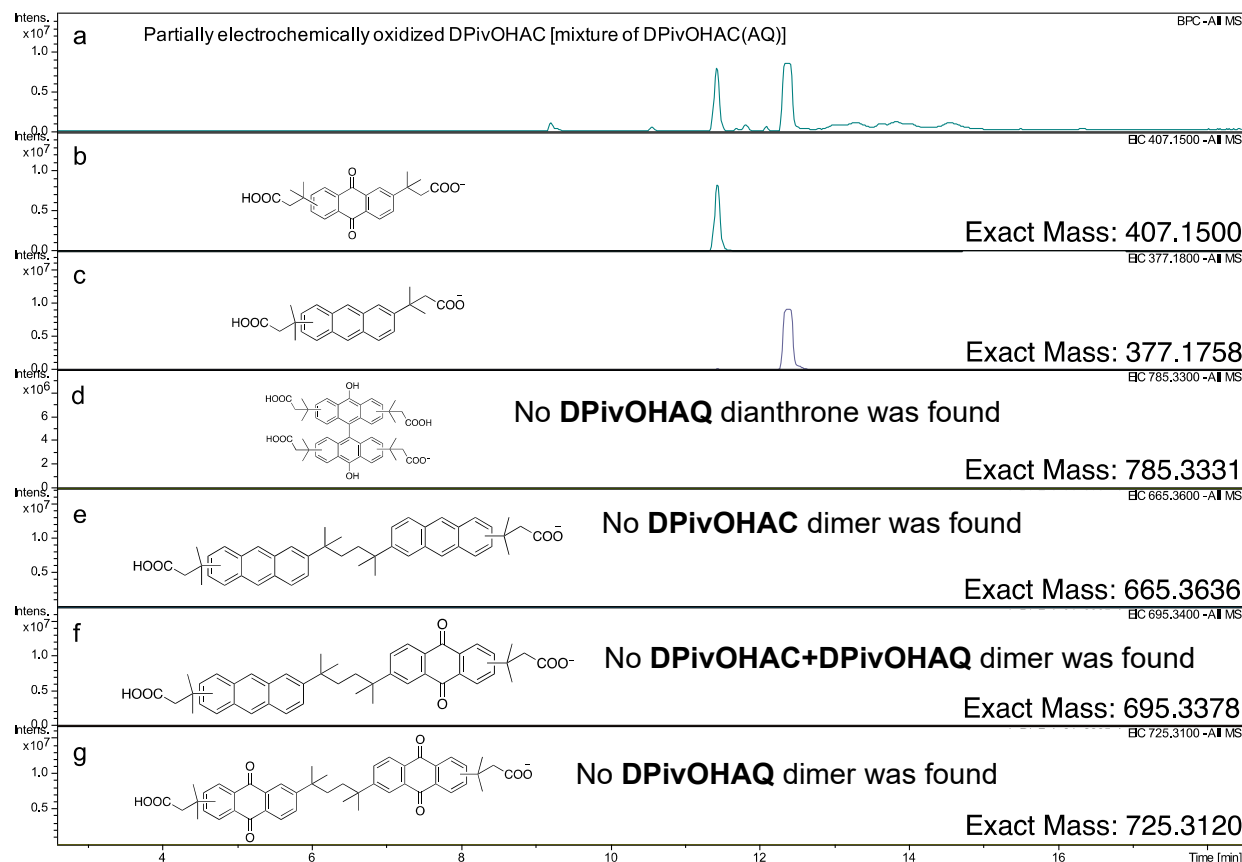
279  
280 Characterization of anolyte: an aliquot (~250  $\mu\text{L}$ ) was transferred from the as-prepared anolyte to  
281 an Eppendorf® tube (capacity: 1.5 mL) and acidified by a drop of concentrated HCl to obtain  
282 **DPivOHAQ** precipitate. The final **DPivOHAQ** precipitate was re-dissolved in  $\text{DMSO}-d_6$  for <sup>1</sup>H  
283 NMR measurement; the yield is 89.0%. The faradaic efficiency (%) = [yield (%)] / 1.2] = 74.2%.



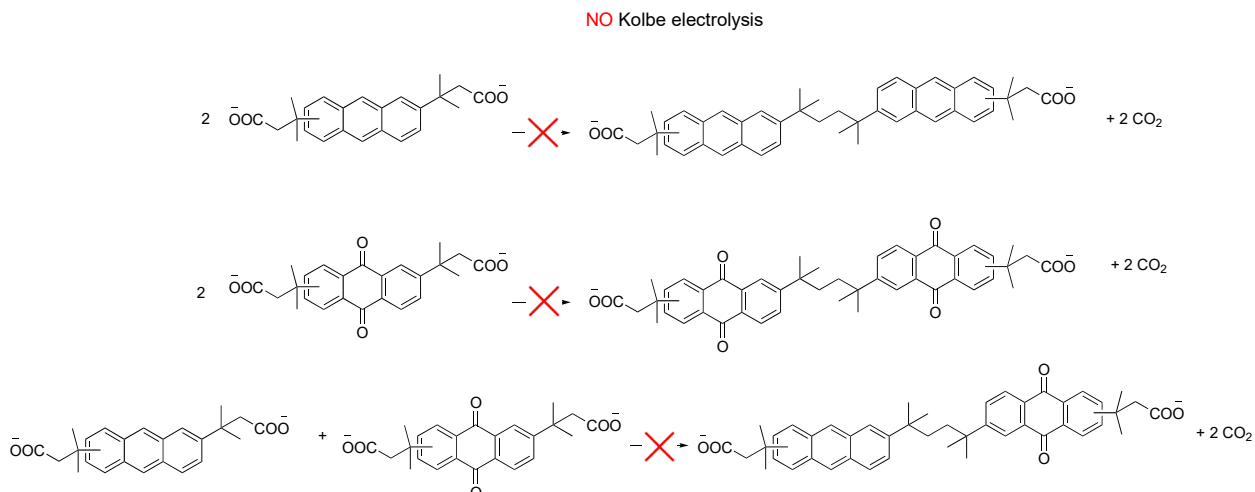
284  
285 **Figure S5.** The electrochemical oxidation of 0.5 M **DPivOHAC(COO<sup>-</sup>)** (**Electrosynthesis IV**).



286  
287 **Figure S6.** <sup>1</sup>H NMR spectrum of **DPivOHAQ** in DMSO-*d*<sub>6</sub> synthesized via the procedure  
288 described in **Electrosynthesis IV**. From the aromatic peak integrations, we found that 89.0%  
289 **DPivOHAQ** was generated (when the two set of peaks at chemical shifts of 7.95 and 8.10 ppm  
290 were integrated), 11.0% **DPivOHAC** was remaining.  
291



292  
293 **Figure S7.** Mass spectra of partially electrosynthesized **DPivOHAQ** (from **Electrosynthesis IV**)  
294 measured by liquid chromatography–mass spectrometry (LC–MS). (a) The peak intensity and  
295 retention time of partially electrosynthesized **DPivOHAQ** under negative mode. (b) The peak  
296 intensity and retention time of **DPivOHAQ** under negative mode. (c) The peak intensity and  
297 retention time of **DPivOHAC** under negative mode. (d) The peak intensity and retention time of  
298 the **DPivOHAQ** dianthrone under negative mode. No peak was found in the given retention time  
299 region, which, in combination with the absence of impurities in the <sup>1</sup>H NMR spectra in Figures 3d  
300 and S6, indicates that no observable **DPivOHAQ** dianthrone was generated during the  
301 electrosynthesis. (e)–(f) The peak intensity and retention time of **DPivOHAQ(AC)**-related Kolbe  
302 electrolysis byproducts under negative mode. No peak was found in the given retention time region,  
303 which, in combination with the absence of impurities in the <sup>1</sup>H NMR spectra in Figures 3d and S6,  
304 indicates that no observable **DPivOHAQ(AC)**-related Kolbe electrolysis byproducts were  
305 generated during the electrosynthesis.



306  
 307 **Scheme S1.** Kolbe electrolysis. Kolbe electrolysis-related byproducts are not expected in our cell,  
 308 as the decarboxylation and dimerization reactions usually require much higher voltages and  
 309 precious-metal-based electrodes.<sup>S1</sup> In our cell, we use carbon electrodes and an applied potential  
 310 of 1.2 V. Additionally, we did not detect any dimer formation from LC–MS measurements.

311  
 312 **Electrosynthesis V.** Electrochemical synthesis of **DPivOHAQ(COO<sup>-</sup>)** in a divided cell at 0.5 M  
 313 concentration with a stoichiometric quantity of hydroxide, against the reduction of ferricyanide.

314  
 315 In a flow cell setup (divided electrolytic cell), unbaked AvCarb HCBA (woven carbon cloth) was  
 316 used as electrodes for both sides; Nafion® 212 was used as the membrane. The high-frequency  
 317 area specific resistance (HF–ASR) was maintained at ~1.45 Ω cm<sup>2</sup> before and after  
 318 electrosynthesis.

319  
 320 Anolyte preparation: 1.89 g **DPivOHAC**, 0.745 g KCl, and 0.567 g KOH were dissolved in  
 321 deionized water to obtain a 10 mL solution containing 0.5 M **DPivOHAC**, 1.0 M KCl, and 1.01  
 322 M KOH. We added the stoichiometric quantity of KOH pellets (1.68 g) (*i.e.*, 6 equivalents relative  
 323 to **DPivOHAC**) into the anolyte over the course of constant current charging.

324  
 325 Catholyte preparation: 16.46 g K<sub>3</sub>Fe(CN)<sub>6</sub>, 7.445 g KCl, and 2.805 g KOH were dissolved in  
 326 deionized water to obtain a 100 mL solution containing 0.5 M K<sub>3</sub>Fe(CN)<sub>6</sub>, 1.0 M KCl, and 0.5 M  
 327 KOH.

328  
 329 Electrochemical oxidation of **DPivOHAC(COO<sup>-</sup>)**: a constant current density (100 mA/cm<sup>2</sup>) was  
 330 applied to the divided electrolytic cell for at most 1.7 hours with a 1.2 V voltage cutoff; when  
 331 either time or voltage reached the limit, the potential was held (1.2 V vs. ferro-/ferricyanide) until  
 332 the current decreased to 12 mA/cm<sup>2</sup>. The number of extracted electrons was ~1.2 times higher than  
 333 the theoretical value.

334  
 335 Characterization of anolyte: an aliquot (~250 μL) was transferred from the as-prepared anolyte to  
 336 an Eppendorf® tube (capacity: 1.5 mL) and acidified by a drop of concentrated HCl to obtain  
 337 **DPivOHAQ** precipitate. The final **DPivOHAQ** precipitate was re-dissolved in DMSO-*d*<sub>6</sub> for <sup>1</sup>H  
 338 NMR measurement; the yield is 81.8%. The faradaic efficiency (%) = [yield (%)] / 1.2] = 68.2%.

339

340 **Formation of dianthrone during electrosynthesis**

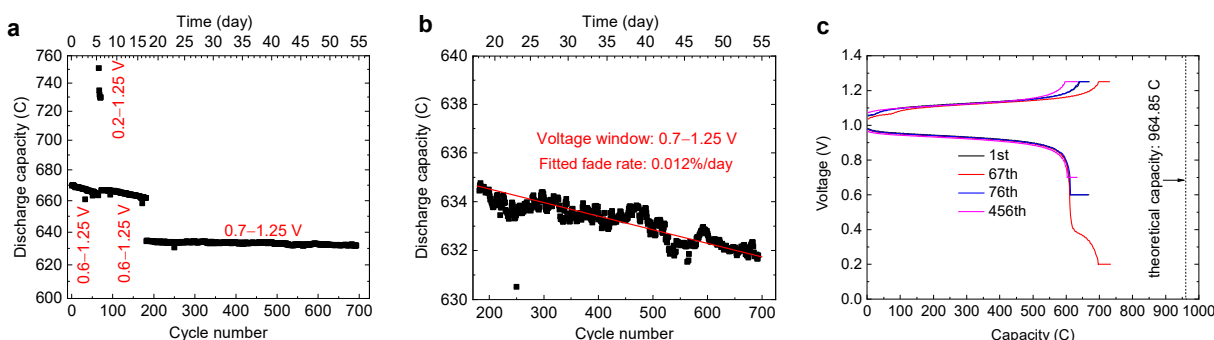
341 Anthrone dimers can be produced during the electrosynthesis when insufficient hydroxide is  
342 present.

343  
344 When there is excess hydroxide in the solution, although some  $\text{OH}^-$  ions will be electrochemically  
345 oxidized to oxygen via the OER, the remaining  $\text{OH}^-$  ions are sufficient for the conversion of  $\text{A}^-$  to  
346  $\text{AQ}^{2-}$ .

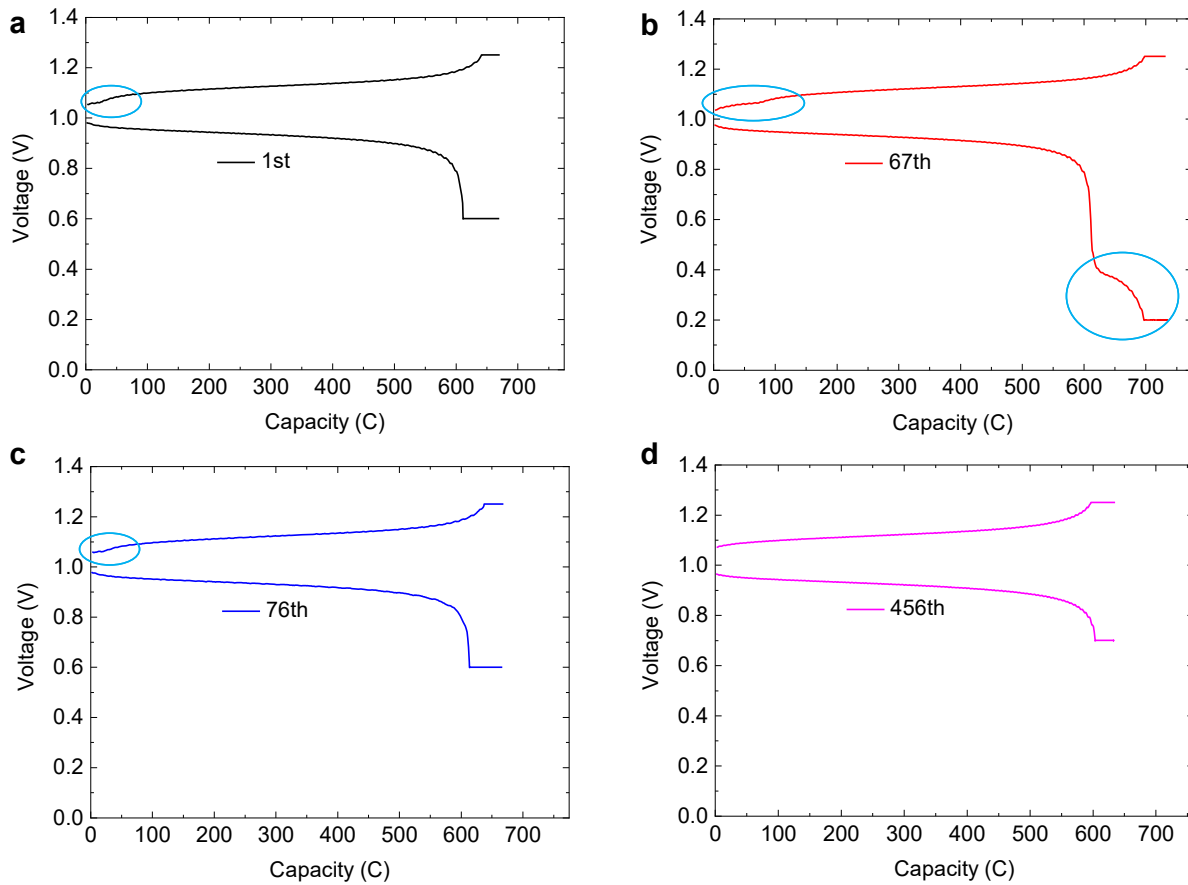
347  
348 When there is no excess hydroxide, given that the OER side reaction is an inevitable competing  
349 reaction, there will be insufficient  $\text{OH}^-$  ions for the conversion of  $\text{A}^-$  to  $\text{AQ}^{2-}$ ; instead, the  
350 anthrone anion  $\text{A}^-$  may be oxidatively dimerized to the dianthrone **DA**. The following figures and  
351 scheme illustrate how **DA** was identified and propose its corresponding electrochemistry.

352  
353 During the electrochemical oxidation of the 10 mL 0.5 M **DPivOHAC(COO<sup>-</sup>)** at pH 12, only 1.68  
354 g of KOH ( $10 \times 0.001 \text{ L} \times 0.5 \text{ M} \times 6 \times 56.1056 \text{ g/mol} = 1.68 \text{ g}$ ) were added to the solution. Although  
355 there is some additional KOH added to the potassium ferricyanide side, hydroxide cannot cross  
356 over to the **DPivOHAC** side of the cell sufficiently rapidly to offset its consumption by  
357 **DPivOHAC** oxidation and the OER.

358



359  
360 **Figure S8.** Cell performance of 0.5 M electrosynthesized **DPivOHAQ** when a stoichiometric  
361 quantity of hydroxide was added into the **DPivOHAC(COO<sup>-</sup>)** solution (Electrosynthesis V). (a)  
362 The long-term cycling performance with adjusted lower voltage cutoffs. (b) The zoomed in  
363 discharge capacity when 0.7–1.25 V voltage cutoffs were applied; the fitted temporal fade rate  
364 was 0.01%/day. (c) The voltage profiles at varying cycle numbers with different lower voltage  
365 cutoffs.

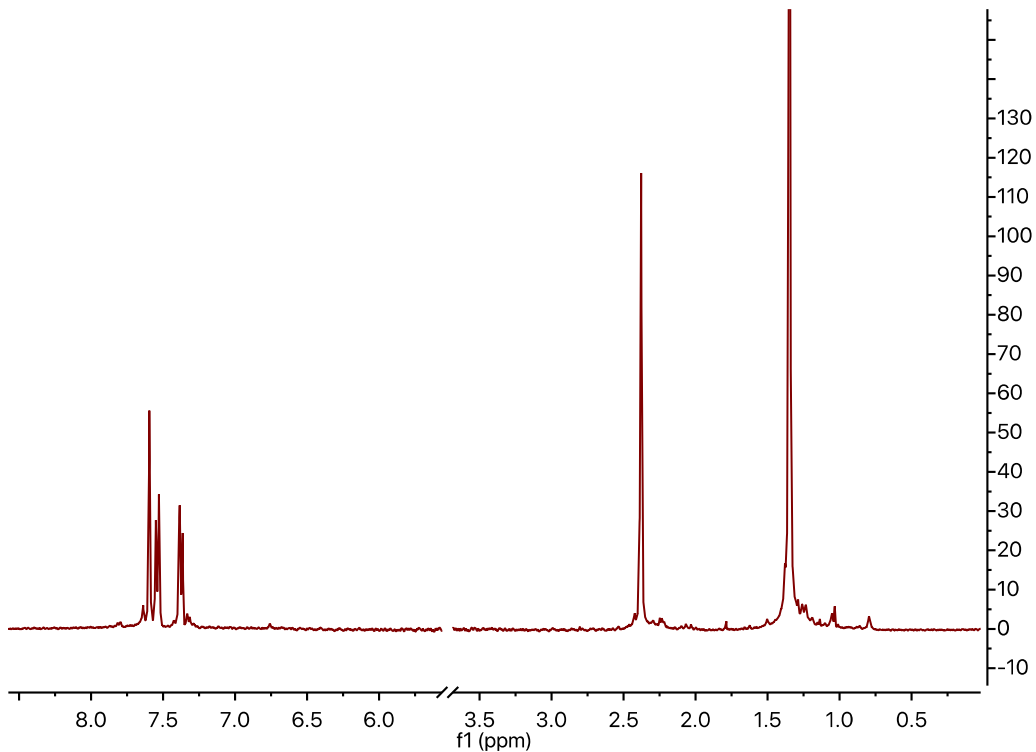


366  
367  
368  
369  
370

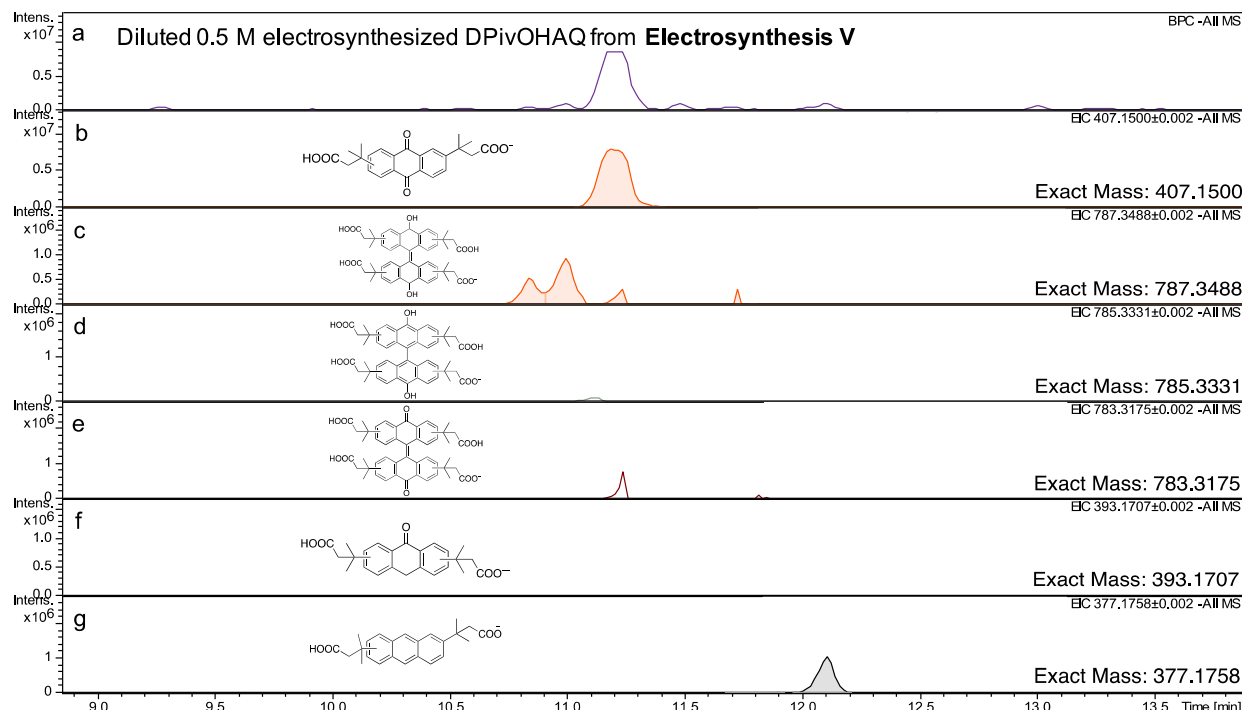
**Figure S9.** Voltage profiles of 0.5 M electrosynthesized **DPivOHAQ** when a stoichiometric quantity of hydroxide was added into the **DPivOHAC** solution (**Electrosynthesis V**) with different lower voltage cutoffs [(a) 0.6, (b) 0.2, (c) 0.6, and (d) 0.7 V]. The upper voltage cutoff is kept constant at 1.25 V for the duration of cell cycling.

371  
372  
373  
374  
375  
376  
377  
378  
379

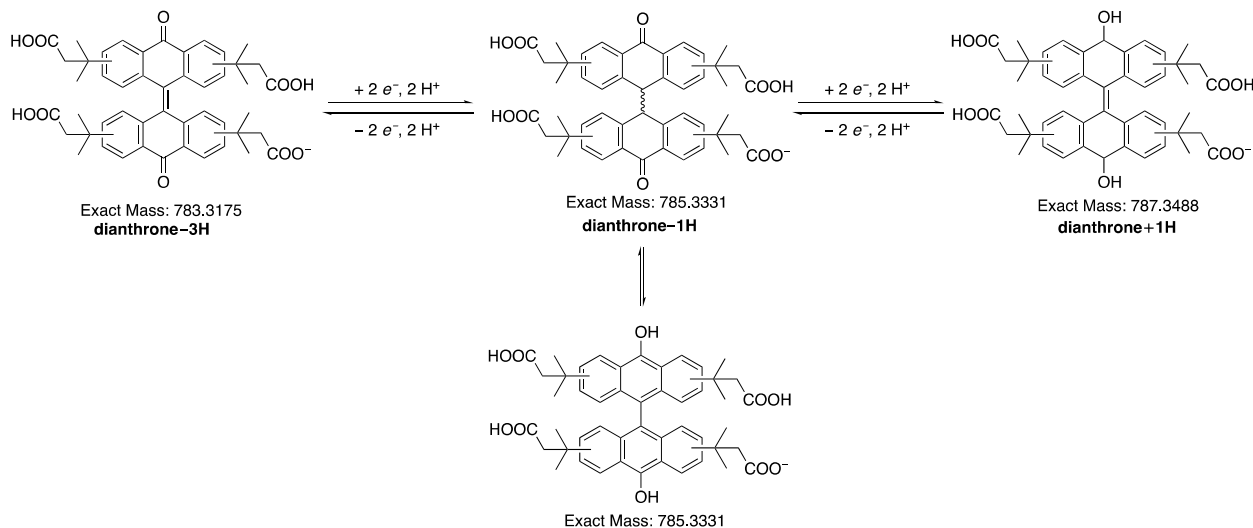
In the 1<sup>st</sup> cycle, the region in (a) circled in cyan shows a small plateau, indicating some redox-active byproducts were produced during the electrosynthesis. In the 67<sup>th</sup> cycle, after lowering the lower cutoff from 0.6 to 0.2 V, we can clearly see the discharge plateau (in the region of 0.2–0.4 V) attributed to byproducts, and the charge plateau attributed to byproducts is also becoming longer. In the 76<sup>th</sup> cycle, after elevating the lower cutoff back to 0.6 V, the shape of the charge profile becomes nearly the same as the one in the 1<sup>st</sup> cycle. After the lower voltage cutoff was further increased to 0.7 V, in the 456<sup>th</sup> cycle, the small plateau attributed to the byproducts disappeared.



380  
381 **Figure S10.**  $^1\text{H}$  NMR spectrum of cycled 0.5 M electrosynthesized **DPivOHAQ** when a  
382 stoichiometric quantity of hydroxide was added into the **DPivOHAC(COO $^-$ )** solution  
383 (**Electrosynthesis V**). The solvent peak was removed to clearly show both aromatic and aliphatic  
384 regions of the cycled **DPivOHAQ** solution. The deuterated solvent is  $\text{D}_2\text{O}$ . The dominating peaks  
385 can be assigned to **DPivOHAQ**. Some small impurity peaks were observed, but they are difficult  
386 to identify. The percentages of side products are very close to the detection limit of the  $^1\text{H}$  NMR  
387 instrument.  
388  
389  
390



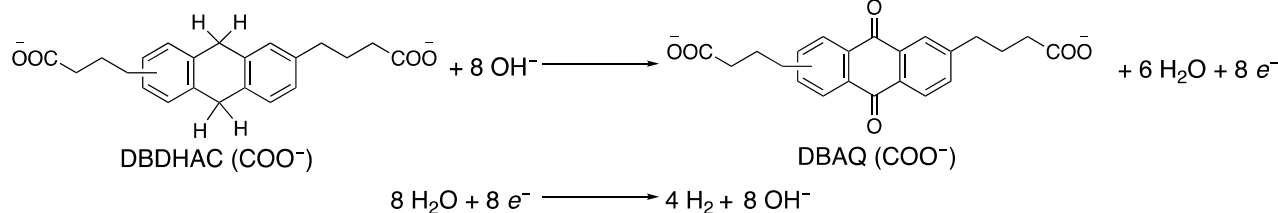
391  
392 **Figure S11.** LC-MS results of cycled 0.5 M electrosynthesized **DPivOHAQ** when a  
393 stoichiometric quantity of hydroxide was added into the **DPivOHAC** solution (**Electrosynthesis**  
394 **V**). (a) The base peak chromatogram of the sample, showing all peaks observed by mass  
395 spectrometry under negative mode. (b) The peak intensity and retention time of **DPivOHAQ-1H**  
396 under negative mode. (c) The peak intensity and retention time of **dianthrone+1H** under negative  
397 mode. (d) The peak intensity and retention time of **dianthrone-1H** under negative mode. (e) The  
398 peak intensity and retention time of **dianthrone-3H** under negative mode. (f) The peak intensity  
399 and retention time of **anthrone-1H** under negative mode (none observed). (g) The peak intensity  
400 and retention time of **DPivOHAC-1H** under negative mode. By integrating the peak areas in (b),  
401 (c), (d), (e), (f) and (g), we found the percentages of **DPivOHAQ** (81.8%), **dianthrone+1H**  
402 (10.2%), **dianthrone-1H** (0.4%), **dianthrone-3H** (1.3%), and **DPivOHAC** (6.3%).  
403



404  
405  
406  
407  
408  
409  
410  
411  
412

**Scheme S2.** Proposed possible redox reactions of dianthrones. Because the **dianthrone+1H** (exact mass: 787.3488) and **dianthrone-3H** (exact mass: 783.3175) were detected and plateaus were observed from the voltage profiles, we propose that there are three redox-active states for the dianthrones.

413  
414



415  
416  
417  
418

An undivided electrolytic cell was prepared with carbon felt (XF30A, Toyobo Co., volumetric porosity: 95%) as the working electrode, a carbon rod as the counter electrode, and Ag/AgCl (3 M NaCl) as the reference electrode.

419  
420  
421  
422

Electrolyte preparation: 0.35 g **DBDHAC** (synthesized by following our previous work), 0.745 g KCl, and 0.561 g KOH were dissolved in deionized water to obtain a 10 mL solution containing 0.1 M **DBDHAC**, 1.0 M KCl, and 1.0 M KOH.

423  
424  
425

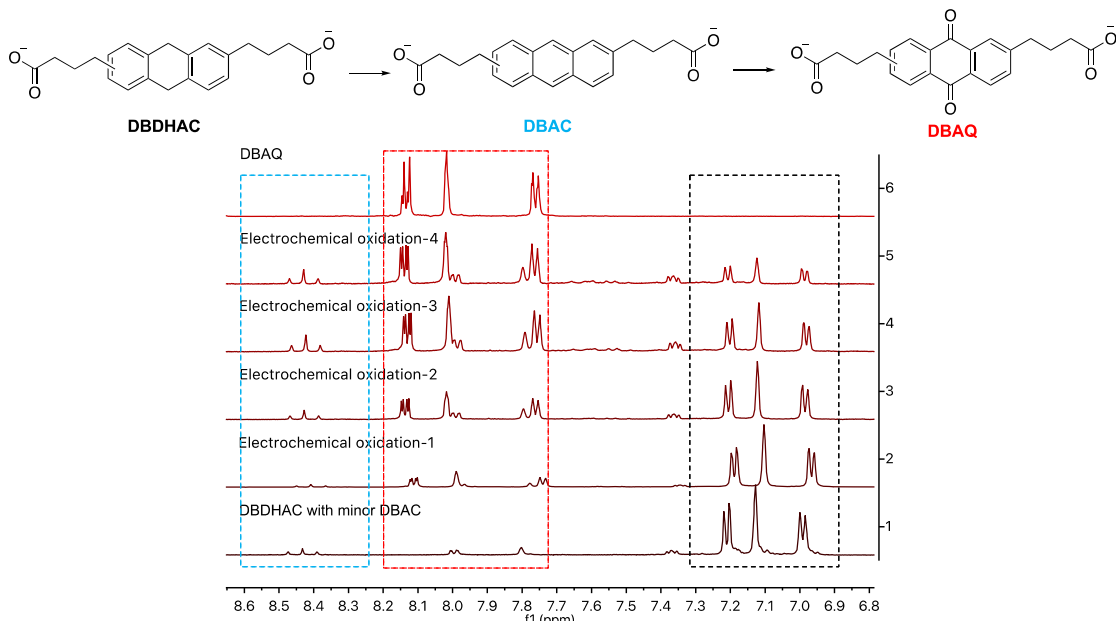
On the working electrode: **DBDHAC** was oxidized to **DBAQ**; on the counter electrode: water was reduced to hydrogen gas.

426  
427  
428  
429  
430

Electrochemical oxidation of **DBDHAC(COO-)**: while the electrolyte was stirring, a constant potential (1.1 V vs. Ag/AgCl) was applied to the divided electrolytic cell until 120% of the required coulombs were extracted from the working electrode. [0.1 M \* 0.01 L \* 96485 C/mol \* 8 \* 1.2 = 926.3 C; 8 electrons need to be extracted from every **DBDHAC** molecule].

431 Characterization of anolyte: an aliquot (250  $\mu$ L) was transferred from the as-prepared anolyte to  
 432 an Eppendorf® tube (capacity: 1.5 mL) and acidified by a drop of concentrated HCl to obtain  
 433 **DBAQ** precipitate. The final **DBAQ** precipitate was re-dissolved in DMSO-*d*<sub>6</sub> for <sup>1</sup>H NMR  
 434 measurement. According to the integration of the <sup>1</sup>H NMR spectrum in the Figure S12, the yield  
 435 is 70%. The faradaic efficiency (%) = [yield (%)] / 1.2] = 58.3%.

436



437

438 **Figure S12.** <sup>1</sup>H NMR spectra of **DBDHAC** (bottom), chemically synthesized **DBAQ** (top), and  
 439 electrochemically synthesized **DBAQ** in an undivided cell after varying extents of reaction.  
 440 **DBDHAC:** 4,4'-(9,10-dihydroanthracene-diyl)dibutanoic acid; **DBAC:** 4,4'-(anthracene-  
 441 diyl)dibutanoic acid; **DBAQ:** 4,4'-(9,10-anthraquinone-diyl)dibutanoic acid. The time interval  
 442 between successive measurements labeled electrochemical oxidation-1, 2, 3, and 4 is  
 443 approximately one hour. The deuterated solvent is DMSO-*d*<sub>6</sub>.

444

#### 445 Light sensitivity experiments

446 It has been reported that quinones and related compounds can decompose in the presence of  
 447 light.<sup>S2-S6</sup> In order to determine the light sensitivity of **DPivOHAQ** and **DBAQ**, we compared  
 448 solutions of each compound held in the presence of and in the absence of light for 1 week. Two  
 449 samples of **DPivOHAQ** (0.1 M, pH 12 in water with 1 M KCl, 1.5 mL each) and two samples of  
 450 **DBAQ** (0.1 M, pH 12 in water, 1.5 mL each) were prepared in separate FEP bottles (VWR Catalog  
 451 No. 16071-008). For each compound, one sample was wrapped in aluminum foil and stored in a  
 452 dark drawer for 1 week. The other sample was held for 1 week under a quartz halogen lamp with  
 453 a controllable output of 50–1000 W set to 500 W (CowboyStudio QL-1000 W HEAD; ePhotoInc  
 454 QL 1000Bulb). The samples exposed to light were allowed to float at the top of a water bath  
 455 containing approximately 16 L of water to dissipate excess heat produced by the lamp (the liquid  
 456 level decreased gradually due to evaporation and was replenished daily). The liquid level was  
 457 maintained at a distance of approximately 20 cm from the light source.

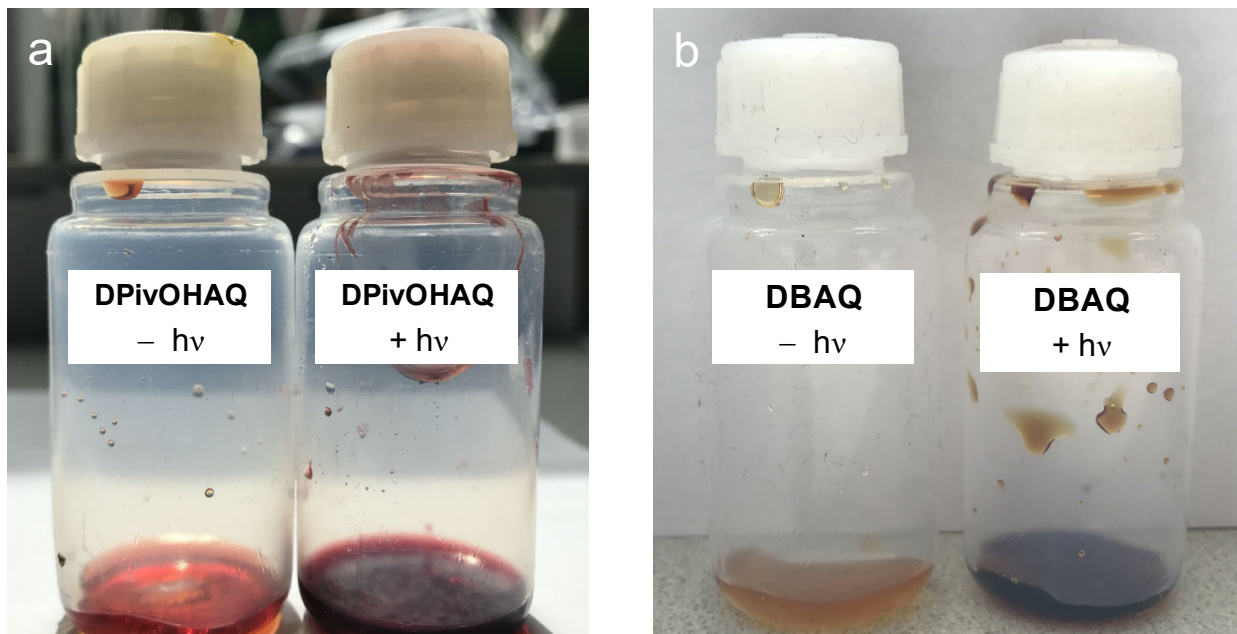
458

459 After 1 week, differences in color were observed between the samples of each compound stored  
 460 in the dark and exposed to light (Figure S13). The formation of a film was also observed in the

461 **DPivOHAQ** sample exposed to light.  $^1\text{H}$  NMR spectra of each sample demonstrate decomposition  
462 of both compounds stored in the presence of light (Figures S14 and S15).

463  
464 We therefore wrapped the electrolyte reservoirs with aluminum foil to avoid decomposition due  
465 to light exposure during cell cycling.

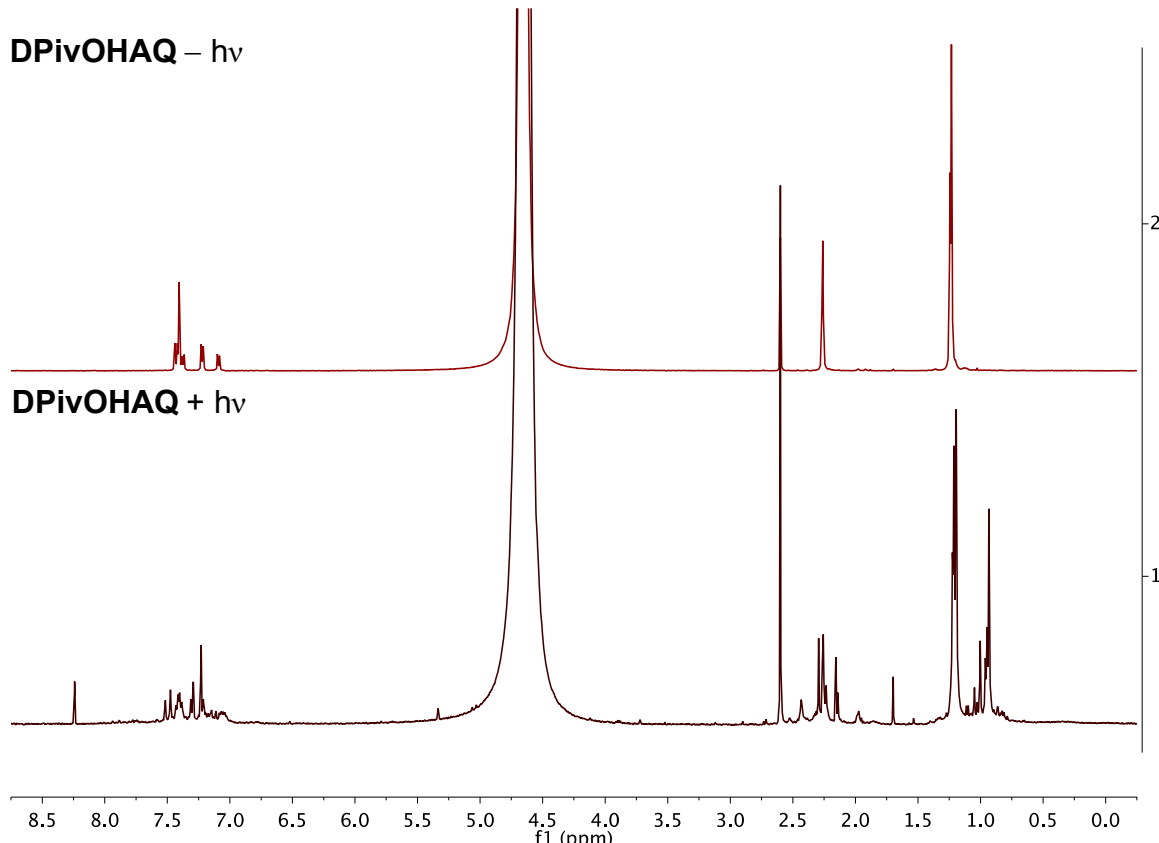
466



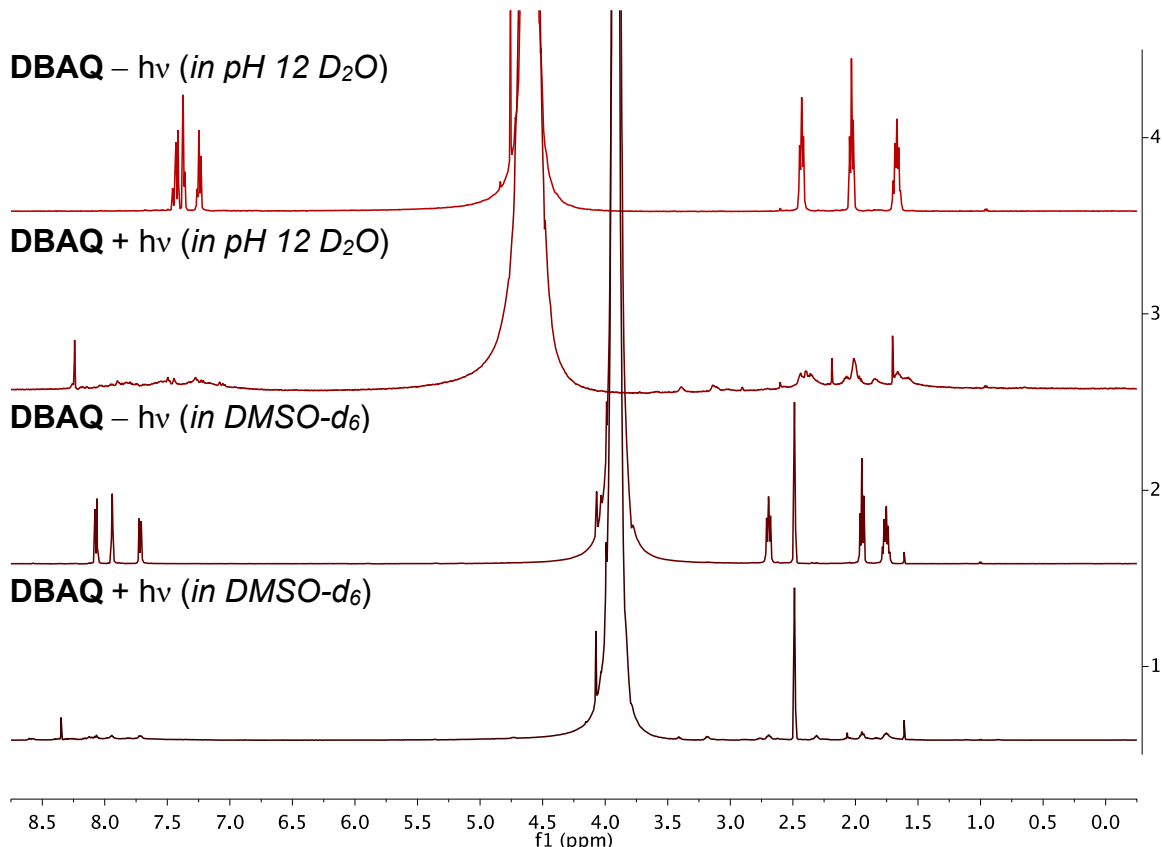
467  
468

469 **Figure S13.** Samples of (a) **DPivOHAQ** (0.1 M, pH 12) stored for 1 week in the absence of light  
470 ( $- \text{h}\nu$ ) and under a 500 W lamp ( $+ \text{h}\nu$ ) and of (b) **DBAQ** (0.1 M, pH 12) stored for 1 week in the  
471 absence of light ( $- \text{h}\nu$ ) and under a 500 W lamp ( $+ \text{h}\nu$ ). Differences in color were observed between  
472 the two samples of each compound. The formation of a film was also observed in the **DPivOHAQ**  
473 sample exposed to light.

474



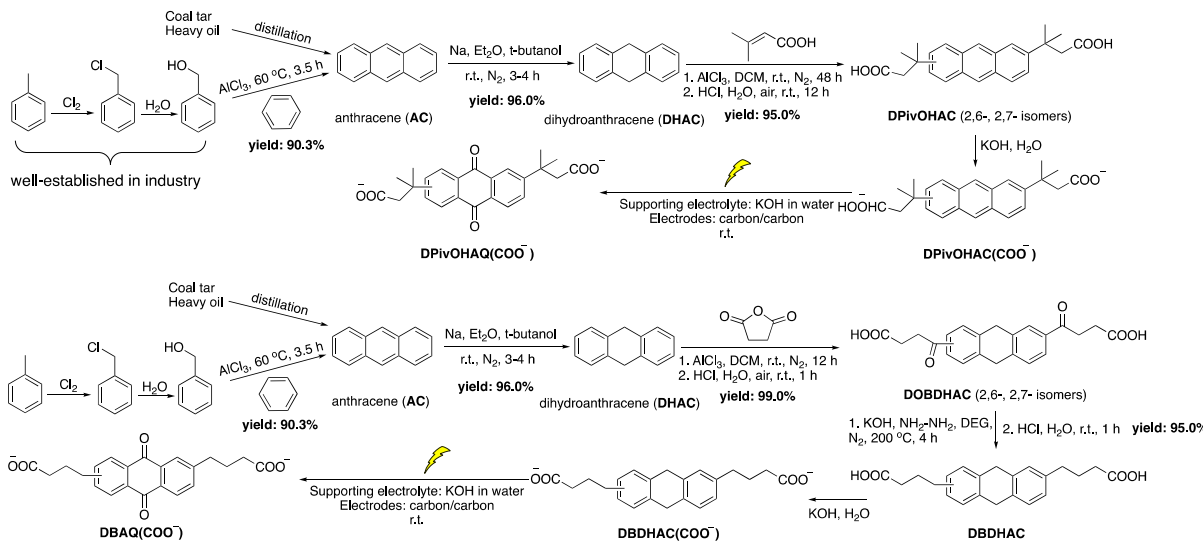
475  
476 **Figure S14.** <sup>1</sup>H NMR spectra of samples of **DPivOHAQ** (0.1 M, pH 12) stored for 1 week in the  
477 absence of light (– hν) and under a 500 W lamp (+ hν), each diluted (1:5.5) in pH 14 D<sub>2</sub>O (1 M  
478 KOD) containing a 9 mM NaCH<sub>3</sub>SO<sub>3</sub> internal standard ( $\delta$  2.6 ppm).



479  
480 **Figure S15.**  $^1\text{H}$  NMR spectra of samples of **DBAQ** (0.1 M, pH 12) stored for 1 week in the  
481 absence of light ( $- \text{h}\nu$ ) and under a 500 W lamp ( $+ \text{h}\nu$ ), each diluted (1:5) in pH 12  $\text{D}_2\text{O}$  or in  
482  $\text{DMSO-}d_6$ .

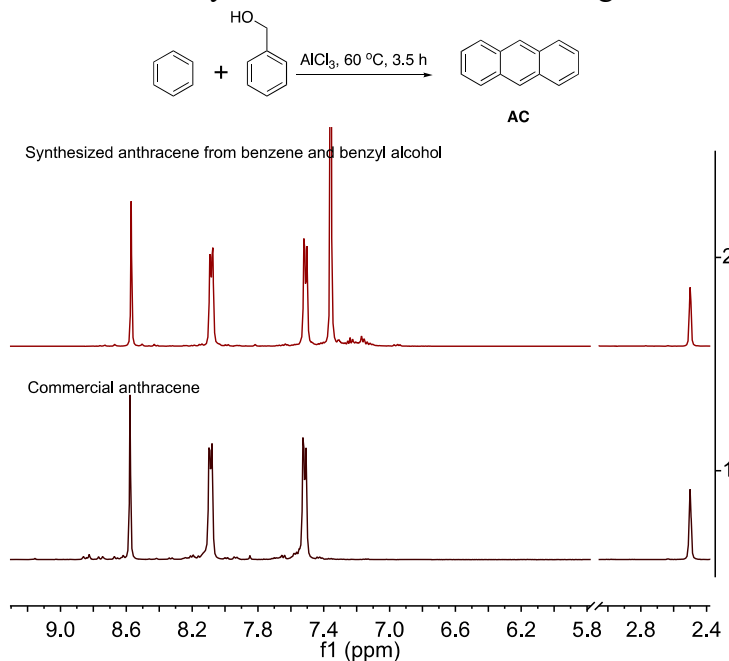
483  
484 **Complete synthesis**  
485

486



487

488 **Scheme S3.** Complete synthetic routes, conditions, and yields of **DPivOHAQ** and **DBAQ** when  
489 commercially available commodity chemicals are used as starting materials.



490

491 **Figure S16.**  $^1\text{H}$  NMR spectra of commercial and synthesized anthracene (**AC**) in  $\text{DMSO}-d_6$ . The  
492 peak at 7.37 ppm in the synthesized **AC** spectrum is from benzene.

493

494

## REFERENCES

495 S1 H.-J. Schäfer, *Topics in Current Chemistry*, 1990, **152**, 91–151.  
 496 S2. G. Maier, L. H. Franz, H.-G. Hartan, K. Lanz and H. P. Reisenauer, *Chemische Berichte*, 1985,  
 497 **118**, 3196–3204.  
 498 S3. B. E. Hulme, E. J. Land and G. O. Phillips, *J. Chem. Soc. Faraday Trans. 1*, 1972, **68**, 1992–2002.  
 499 S4. S. A. Carlson and D. M. Hercules, *Analytical Chemistry*, 1973, **45**, 1794–1799.  
 500 S5. D. M. Hercules, S. A. Carlson, *Analytical Chemistry* 1974, **46**, 674–678.  
 501 S6. A. D. Broadbent, R. P. Newton, *Canadian Journal of Chemistry* 1972, **50**, 381–387.